UNIVERSIDADE DE LISBOA
FACULDADE DE CIÊNCIAS
DEPARTAMENTO DE FÍSICA

Fully non-invasive pressure drop measurements and post treatment prediction in congenital heart diseases via cardiac magnetic resonance and computer flow dynamics

Rita Dias Cabrita Alves

Mestrado Integrado em Engenharia Biomédica e Biofísica
Perfil em Sinais e Imagens Médicas

Dissertação orientada por:
Prof. Nuno Matela, FCUL
Joao Fernandes, DHZB

2017

Resumo

De acordo com os dados de 2017 da Organização Mundial da Saúde, as doenças cardiovasculares são a principal causa de morte a nível mundial. Se estes tipos de doenças não forem diagnosticadas e tratados atempadamente, podem levar a insuficiências cardíacas ou outras complicações irreversíveis.

As duas doenças cardiovasculares congénitas estudadas neste trabalho são a coarctação aórtica (CoA), caracterizada por uma estenose, habitualmente, na zona do arco da artéria aorta, e a doença da válvula aórtica (AvD), uma malformação ao nível da válvula aórtica. Estas doenças são responsáveis por cerca de 50,000 intervenções por ano. Deste modo, a melhoria métodos de diagnóstico e de intervenção adequados e eficientes é uma prioridade e pode levar ao decréscimo no número das intervenções, bem como reduzir a morbilidade e a mortalidade.

A área de imagiologia médica de diagnóstico tem tido uma evolução significativa ao longo dos anos e é de extrema importância nas tentativas de substituição de métodos de diagnóstico invasivos. As imagens médicas são adquiridas e posteriormente processadas e analisadas, com recurso a programas adequados. Atualmente, é possível obter os valores de gradientes de pressão relativa a partir de Ecocardiografia Doppler e Ressonância Magnética. Contudo, os gradientes de pressão medidos no cateterismo cardíaco, o método *gold standard* para o diagnóstico de CoA e AvD, são gradientes de pressão absoluta. Nesta dissertação desenvolveu-se um método de diagnóstico de CoA e AvD, a partir dos mapas de pressão relativa no estreitamento da aorta e na válvula aórtica, respectivamente.

O método matemático desenvolvido tem por base as equações de Poisson, resolvida com a condição de fronteira de Neumann utilizando os métodos de elementos finitos, e a de Navier Stokes para a conservação do momento. O método desenvolvido também tem em conta a informação proveniente da função de Windkessel da artéria aorta, uma artéria distensível. Esta função dá-nos o comportamento da propagação do pulso de pressão com uma velocidade de pulso de propagação. Deste modo, é observado um desfasamento temporal entre as curvas de fluxo da pressão e da velocidade, entre as duas regiões de interessante escolhidas. Deste modo, o método, denominado de Time-shift Corrected Pressure Maps (TCPM, sigla em inglês), permite obter os mapas de pressão absoluta, isto é, mapas de pressão que têm em conta o intervalo de tempo entre os picos de pressão na aorta descendente e ascendente, no caso do primeiro estudo, e antes e depois da válvula aórtica, no caso do segundo estudo. Os pacientes de ambos os estudos tinham indicação clínica para cateterismo cardíaco e foram submetidos a ressonância magnética cardiovascular de contraste de fase em tempo real (4D PC MRI, em inglês), para recolher as imagens ao nível da aorta e da válvula aórtica e os respectivos campos de velocidade da corrente sanguínea.

O primeiro estudo tem como objetivo a aplicação do método TCPM a 27 pacientes de CoA (n=16 masculinos, n=11 femininos, faixa etária de 4 a 52 anos, idade média de 20±15 anos). Após aquisição das imagens, estas foram processadas usando programas específicos. Em primeiro lugar foi necessário segmentar a aorta, seguiu-se a seleção das regiões de interesse e, finalmente, a obtenção dos campos de velocidade e dos mapas de pressão relativa entre as duas regiões de interesse selecionadas. Após aplicação do método TCPM, foram aplicados testes estatísticos (correlação, teste t e Bland-Altman) para comparar os valores obtidos a partir de TCPM com os valores obtidos no cateterismo cardíaco. Após processamento das imagens dos 27 pacientes, 6 pacientes foram retirados do estudo. N=3 pacientes foram retirados porque a percentagem de fluxo que passa pelo estreitamento é insuficiente para calcular o gradiente de pressão a partir de TCPM e N=3 pacientes foram retirados porque a aorta não estava inserida por completo no FOV. As medições obtidas a partir de TPCM e cateterismo cardíaco têm uma correlação linear significante (R^2=0,90; p<0,001). A partir dos gráficos Bland-Altman é possível verificar uma boa concordância entre as medições de ambos os métodos, com bias de -2,69 mmHg e os limites de concordância de ±4,74 mmHg. O teste de equivalência mostrou uma relação significante entre os métodos (p=0,007).

O segundo estudo tem como objetivo a aplicação do método TPCM e o método da Área de Gorlin a 4 pacientes de AvD (n=4 masculinos, faixa etária 17 a 36 anos, idade média 27±7 anos). O método da Área de Gorlin permite obter o gradiente de pressão absoluta a partir da área geométrica da válvula e do fluxo total que passa nessa área. Após a aquisição das imagens, foi feito o processamento das mesmas. Numa primeira fase, as imagens foram segmentadas na região da válvula aórtica. Depois, as imagens segmentadas foram analisadas em dois programas distintos. O primeiro foi utilizado de forma a obter os campos de velocidade e os mapas de pressão relativa entre dois pontos antes e depois da válvula aórtica. O segundo permitiu definir a região da válvula como região de interesse e exportar os valores de velocidade, área, pressão relativa e fluxo absoluto nessa região. Os resultados mostram uma correlação linear significativa entre os valores de cateterismo cardíaco e de TCPM (R^2=0,99; p<0,001). Os gráficos de Bland-Altman mostram uma boa concordância entre os valores de TCPM (24,75±22,50 mmHg) e de cateterismo (20,88±19,51 mmHg), com um bias de -3,87 mmHg e limites de concordância de ±3,64 mmHg. Os resultados também sugeriram uma ligeira subestimação dos valores do cateterismo cardíaco a partir do método da Área de Gorlin (14,47±13,00 mmHg), com um bias de 6,41 mmHg e limites de concordância de ±7,15 mmHg. Este estudo foi feito com uma amostra diminuta de 4 pacientes, o que não é suficiente para retirar conclusões com significância. Contudo, foi uma primeira abordagem positiva, que mostra a potencialidade que este método pode vir a apresentar.

O método TCPM proposto neste projeto permite a medição não invasiva de gradientes de pressão absoluta a partir de mapas de pressão relativa em pacientes de CoA e AvD. Vários aspectos têm que ser tidos em conta de forma a garantir a eficácia deste método. Por exemplo, as regiões de interesse escolhidas têm que se cuidadosamente selecionadas de forma a serem perpendicular à direção do fluxo naquele local. Só desta maneira é possível obter o fluxo, os campos de velocidade e as pressões relativas corretas. Também, se o raio da estenose for menor que 2 voxéis, a relação sinal-ruído aumenta substancialmente, e a resolução especial da aquisição é insuficiente. Contudo, a aplicação do método TPCM a casos de grande estreitamento não é necessária visto que estes casos já são tipicamente identificados em imagens anatómicas de ressonância magnética e que o paciente segue automaticamente para intervenção quando a área do estreitamente representa cerca de 50% do valor de área típico da aorta.

O método não invasivo TCPM apresenta uma boa concordância com o cateterismo cardíaco em termos da medição dos gradientes de pressão em CoA e AvD. Os bias e os limites de concordância entre cateterismo e TCPM foram substancialmente mais pequenos que os bias e os limites de concordância entre cateterismo e ecocardiografia Doppler e entre o cateterismo e o método da Área de Gorlin. Com os resultados apresentados já é possível ver o potencial desta técnica no processo de diagnóstico e decisão de intervenção em casos de CoA e AvD. Contudo, estudos com populações maiores será extremamente benéfico para validar clinicamente este método.

Palavras-Chave: Ressonância Magnética Cardiovascular, Coartação da Aorta, Gradientes de Pressão, Estenose Aórtica, Mapas de Pressão através de Ressonância Magnética, 4D PC-MRI.

Abstract

This dissertation aims to validate MRI-based time-shift corrected pressure mapping (TCPM) against cardiac catheterization in CoA and AvD patients. Also, in AvD patients, catheterization will be compared against Gorlin Area method. This project is divided in two independent studies: the first one for CoA patients and the second one for AvD patients, all with clinical indication for cardiac catheterization.

In both CoA and AvD, clinical guidelines recommend treatment in the presence of a relevant pressure gradient. While reliable non-invasive measurement approaches would be crucial, the accuracy of currently available methods has been limited.

In both studies, 4D PC-MRI was performed to compute relative pressure maps via Pressure-Poisson equation. To consider the patient-specific peak pressure time-shift from the ascending to the descending aorta and before and after the aortic valve, relative pressure gradient maps were corrected by the inertial term. Comparison between TCPM and invasive peak-to-peak measurements was performed using correlation, Bland-Altman plots and mean-equivalence t-test.

In the first study, with a cohort of 21 patients with CoA, TCPM and catheter measurements showed significant linear correlation (R^2=0.90; $p<0.001$). Bland-Altman plots demonstrated good agreement between TCPM and catheter derived pressure gradients with mean differences of -2.69 mmHg and 95% limits of agreement between -6.38 and 1.00 mmHg between methods. The mean-equivalence test was significant (p=0.007).

In the second study, with a cohort of 4 patients with AvD, the catheterization measurements were compared against TPCM measurements. The results showed significant linear correlation (R^2=0.99; $p<0.001$). Bland Altman plots showed a good agreement between TCPM (24.75±22.50 mmHg) and catheter derived peak-to-peak pressure gradients (20.88±19.51 mmHg), and suggested slight underestimation of the pressure gradients by the Gorlin Area method (14.47±13.00 mmHg).

Non-invasive TCPM showed equivalence to pressure gradients from invasive heart catheterization in patients with CoA and AvD. However, in the AvD study, they were obtained for a very small cohort of patients and do not have sufficient statistical significance to validate the method for AvD patients.

Key Words: Cardiac Magnetic Resonance Imaging, 4D PC-MRI, coarctation of aorta, pressure gradient; aortic valse disease; MRI pressure mapping;

Contents

Acknowledgements

I would like to express my sincere gratitude to both my supervisors Prof. Nuno Matela and João Fernandes, for the support and patience throughout this whole year.

Thank you to all the team members from DHZB that accompanied me during the internship and that taught me things I will take with me for the rest of my life. João Fernandes, Tiago Silva and Alireza Khasheei, it was a pleasure to share the same workspace, to avoid dinner and to talk about the future with all of you (despite my morning mood).

To all the professors from the Institute of Biophysics and Biomedical Engineering my sincere thanks for all the knowledge you shared with me and my colleagues. You are the main reason why we all have such great opportunities and hope no one did disappoint you.

Without the constant support of my friends this thesis would not be a reality. To “Pessoal Fixolas” the biggest “Thank you!” of the world. You were responsible for keeping me happy and grounded while away from everything I knew. A special thanks to Tatiana Costa, Marta Carrilho, Filipe Costa and Tânia Gonçalves for enjoying Berlin with me, enduring the cold and the never-ending tour I prepared, for making me eat breakfast, for the snow fights and for the birthday I thought I could never have. To my favourite “Berliners”, Andreia, Christina, Iara, Julia, Katherine, Leonor, Patrick, Rita, Selin and Tobias, thank you for teaching me so much about your culture and for making Berlin feel like home.

My family was crucial for all of this. My parents were the biggest supporters of this whole adventure, not only this last year, but since I was born. Thank you for allowing me and Jorge to fly away but also for remind us where home is. My brother, the biggest example that inspires me every day to dream and to not be afraid of trying anything I set my mind into. And finally, my grandmothers, my personal heroes, that motivate me to work hard but enjoy life to the maximum. Your soup was missed in those 10 months I lived abroad.

This thesis is an accomplishment. And I am lucky that I have this great group of people surrounding me and celebrating with me this new phase of my life. Thank you! Obrigada! Vielen Dank!

List of Figures

List of Tables

List of Abbreviations

AV – Aortic Valve
AvD – Aortic Valve Disease
AVR – Aortic Valve Regurgitation
AVS – Aortic Valve Stenosis
CHD – Congenital Heart Diseases
CoA – Coarctation of the Aorta
CT – Computer Tomography
FA – Flip Angle
FOV – Field of View
LA – Left Atrium
LV – Left Ventricle
MRI – Magnetic Resonance Imaging
PC – Phase Contrast
ROI – Region of Interest
RV – Right Ventricle
SE – Spin-Echo
TE – Echo Time
TOST – Two One-Sided Test
TR – Repetition Time
VC – Vena Contracta
VENC – Velocity Encoded

Motivation

According to the World Health Organization, cardiovascular diseases (CVDs) are the principal cause of death globally. CVDs are a group of disorders of the heart and blood vessels and can lead to irreversible heart complications [1]. Congenital Heart Diseases are diseases that occur when the heart and the blood vessels near the heart do not develop normally before birth. In this dissertation, the two diseases discussed are coarctation of the aorta (CoA) and aortic valve disease (AvD). Catheterization is the gold standard for diagnosis and intervention, for both diseases. Catheterization is an invasive procedure that could lead to: bleeding, infection and bruising at the catheter insertion site; blood clots, which may trigger a heart attack; damage to the artery where the catheter was inserted, or damage the arteries as the catheter travels through the body. To provide adequate prognosis and treatment and avoid the need of an invasive examination to detect these diseases, it is necessary an approach to improve diagnosis.

While non-invasive diagnostic methods would be preferable, cardiac catheterization is still seen as the clinical reference standard for CoA and AvD evaluation at many centres. However, current noninvasive methods are unsatisfactory, since they are highly inaccurate [1, 2]. For example, cuff based measurements provide pressure differences between peripheral arteries and are affected by anatomic variation, pulse wave velocities, measurement setting and cuff-size [2,3]. Doppler echocardiography applies a simplified Bernoulli equation, which tends to overestimate the pressure gradient, since maximal velocities across the stenosis are increased due to higher wall stiffness and presumes the presence of an ideal fluid [4, 5].

Four-dimensional velocity encoded MRI (4D-VEC MRI) was shown to be able to map the relative pressures in one vessel [6]. Although relative pressure maps do not take into account the time shift parameter that invasive peak-to-peak measurements take, manual corrections, by adding single cuff measurements and a standard pressure curve, have been suggested [7].

The aim of this dissertation is to demonstrate a novel method of non-invasive MRI-based time-shift corrected pressure mapping to assess pressure gradients and to validate it against peak-to-peak pressure differences obtained from invasive heart catheterization. This method will also be compared against other commonly used non-invasive measurements, such as measurements based on cuff pressures and Doppler echocardiography.

1. Background Material

1.1. Cardiovascular Structures of Interest

1.1.1. Left Ventricle

The Left Ventricle (LV) is the structure that receives blood from the Left Atrium (LA) and pumps it to all the tissues of the body, through the aorta. Most of the left lateral surface of the heart is formed by the LV. Also, it forms part of the inferior and posterior surfaces. The wall of the LV is characterized by *trabeculae carneae* (also referred as "beams of meat") which are rounded or irregular muscular columns. Comparing the LV to the Right Ventricle (RV), the muscular columns tend to be relatively thinner and the myocardium in the wall of the LV is much thicker (Figure 1) [8].

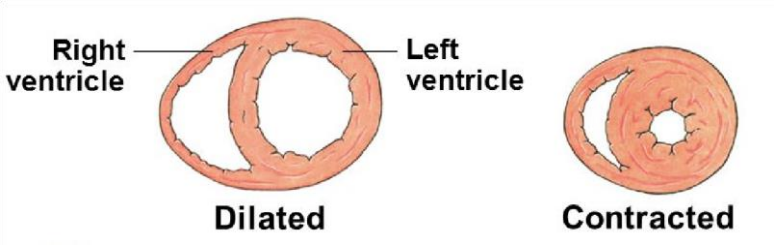

Figure 1 - Comparison between left ventricle and right ventricle in terms of shape and myocardium thickness in dilated and contracted moments [101].

1.1.2. Aorta

The aorta is the largest artery in the body. It can be divided in three main sections: the ascending aorta, which supplies the arms and head, the descending aorta, which supplies the lower part of the body, and the aortic arch that connects the ascending section to the descending section. The aortic arch has an inverted U form and is the origin of three major arteries: left subclavian artery, left common carotid artery and brachiocephalic artery (Figure 2) [2]. The aorta is of absolute importance since every major organ, except the liver, is supplied by arteries that arise from the aorta [9].

Since the structure of the aorta contains a high density of elastic fibers, it can tolerate the pressure changes characteristic of the cardiac cycle. During LV systole, pressures rise rapidly and aorta expands. When the pressure drops in LV diastole, the elastic fibers recoil to their original dimensions. This recoil slows the pressure drop in the adjacent vessels during LV diastole. Therefore, the wall characteristics of the elastic arteries are the main reason for the absence of pressure oscillations when the blood reaches the arterioles in healthy subjects.

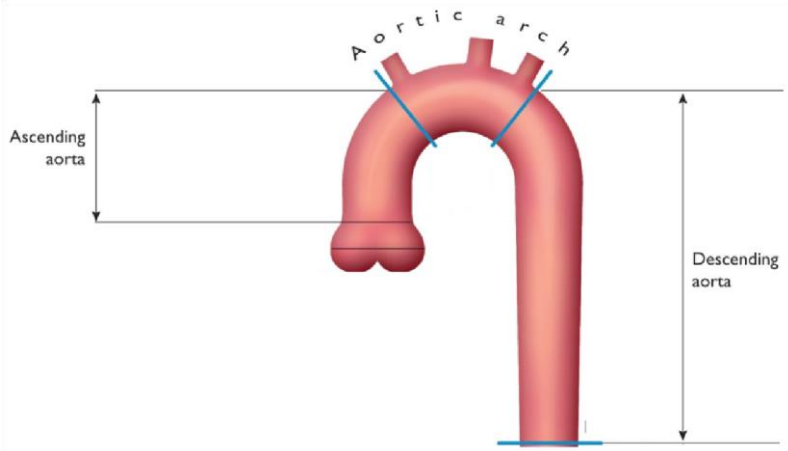

Figure 2 - Aorta and its division in three parts: ascending aorta, aorta arch and descending aorta. Adapted from [2].

1.1.3. Aortic Valve

The aortic valve (AV) is one of the semilunar valves of the heart. Semilunar refers to the shape of the valve cups visible in a frontal section of the heart. The AV is the site where the aorta joins the LV (Figure 3). This valve is responsible for the controlled blood flow from the LV to the aorta. It is compose by three leaflets, although approximately 2% of the population has congenitally two leaflets [10].

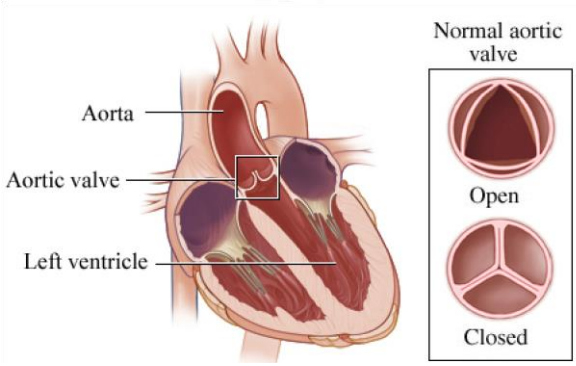

Figure 3 - Position of the aortic valve in between the left ventricle and the aorta. Schematic behavior of the aortic valve in the moments open and closed. [99]

1.2. Cardiovascular Diseases of Interest

1.2.1. Coarctation of the Aorta

CoA is a narrowing of the aorta and is one of the most common diseases in the aorta, accounting for 5-8% of all congenital heart diseases (CHD) (Figure 4) [11]. Due to its location, CoA can have different definitions: if it is located less than 10mm from the origin of the left subclavian artery it is defined as proximal CoA; if it is located more than 10mm from the origin of the left subclavian artery it is defined as distal CoA [12].

CoA has clinical features that include upper body systolic hypertension and lower body hypotension, creating a blood pressure gradient between upper and lower extremities. The blood pressure gradient is the main diagnostic factor for CoA [13].

This disease can be mild or severe. It is considered that a CoA is severe if the pressure gradient across the narrowing is equal or higher than 20 mmHg and mild if the pressure gradient is less than 20 mmHg. In cases of severe CoA the patient is submitted to surgery. There are various surgery options such as stents and balloon angioplasty [14].

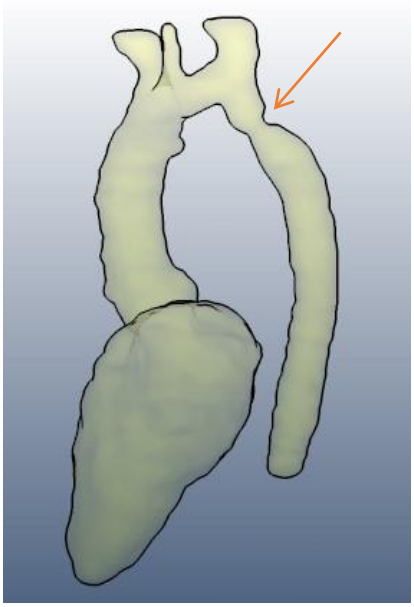

Figure 4 – Left Ventricle and Aorta of a 10 years old patient with CoA. The narrowing is indicated with a red arrow.

1.2.2. Aortic Valve Disease

AvD is one of the most common and most serious valve disease problems. There are two main types of aortic valve disease: Aortic Valve Stenosis, when the AV opening is narrowed, which prevents it from opening fully and obstructs blood flow, and Aortic Valve Regurgitation, when the AV does not close properly, which allows blood to flow backward into the LV. It can occur because of calcification and congenital valvular defects such as bicuspid AVs or rheumatic disease (Figure 5) [15].

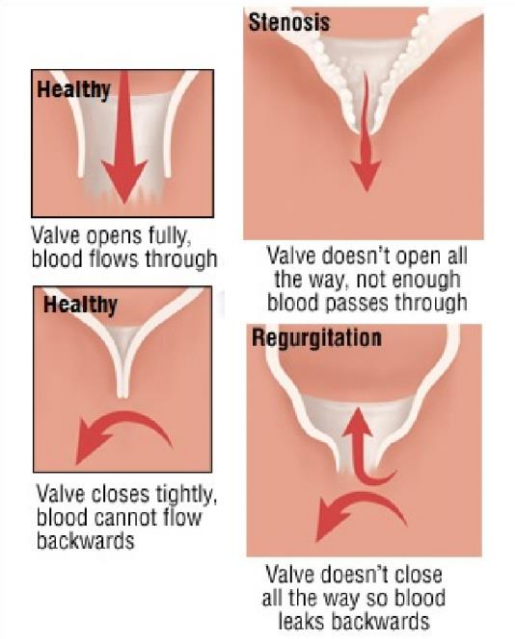

Figure 5 - Comparison between a healthy valve and valves with Aortic Valve Disease.

Due to the modified blood flow in and out of the heart, the LV needs to work more intensively to pump the blood through the AV. This can lead to a remodel of the shape of the LV and may also affect the pressure in the LA [16].

Aortic Valve Stenosis (AVS) and Aortic Valve Regurgitation (AVR) can be characterized based on their severity. The clinical guidelines to characterize each disease are present in the following tables 1 and 2:

Table 1 - Recommendations for classification of Aortic Valve Stenosis severity according to European Society of Cardiology [24].

	Mild	**Moderate**	**Severe**
Aortic Jet Velocity (m/s)	2.6 – 2.9	3.0-4.0	>4.0
Mean Gradient (mmHg)	<30	30-40	>40
Aortic Valve Area (cm2)	>0.85	0.60-0.85	<0.6
Velocity ratio (cm2/m2	>0.50	0.25-0.50	<0.25

Table 2 - Quantitative parameters for Aortic Valve Regurgitation classification according to European Society of Cardiology [6].

	Mild	**Moderate**	**Severe**
Regurgitant Volume (mL/beat)	<30	30-59	[3]60
Regurgitant Fraction (%)	<30	30-49	[3]50
Effective Regurgitant Orifice	>0.85	0.10-0.29	[3]0.30

For AVR patients, intervention is recommended when ejection fraction ≤50% and when there is LV enlargement with an LV end-diastolic diameter (LVEDD) >70 mm or left ventricular endsystolic diameter (LVESD) >50 mm. For patients close to these intervention thresholds, it is advised close follow. In asymptomatic patients, regular assessment of LV function and physical condition are crucial to identify the optimal time for surgery. A rapid progression of ventricular dimensions or decline in ventricular function on serial testing is a reason to consider surgery [17].

For AVS patients, intervention is recommended for patients with severe AVS and DP ≥ 40 mmHg. The only exceptions are patients with severe comorbidities indicating a survival of less than a year and patients whom would be unlikely to get an improved quality of life from the intervention. Initial diagnosis of AVS typically is obtained during routine physical examination with the presence of a heart murmur or other abnormal sounds. Undiagnosed subjects can experience severe symptoms like angina or heart failure [18].

1.3. Basic Principles of Cardiac Magnetic Resonance Imaging

Cardiac Magnetic Resonance (MRI) is the Magnetic Resonance Imaging when applied to the heart and main blood vessels and uses Magnetic Resonance sequences optimized for the

cardiovascular system. It is a well-established method to analyze the anatomy and pathophysiology of the cardiovascular system, and therefore is also an alternative method of diagnosis and decision making on cardiovascular diseases.

One of the biggest technical challenges that MRI must overcome is the rapid and complex motion of the heart. Also, effects of respiratory motion and systolic ventricular blood velocities (that can reach 500cm/s in certain pathologies) have to be taken into account [19]. To generate images free of motion artifacts, the images are acquired quickly, using or improved scanners, that allow faster gradients, or rapid imaging techniques, such as parallel imaging [20]. Furthermore, breathhold techniques are also used. Typical MRI parameters are: field of view (FOV) 350 x 350 mm^2, repetition time (TR) = 2.8 ms, echo time (TE) = 1.4 ms, acquired voxel size = 2.2 x 2.2 x 8 mm^3, flip angle (FA) = 60ºand reconstructed voxel size = 1.3 x 1.2 x 8 mm^3.

The orientation of the heart within the chest varies from patient to patient and this variable makes the localization of the images unpredictable. Most of the cardiac imaging techniques use cardiac axes, which need to be identified for each individual patient. A full-chest sequence is necessary as localizer and after these, various sequences are planned such as transverse, sagittal and coronal.

Pulse sequences are programed to encode the timing and magnitude of the pulses emitted by the MR. Spin-echo (SE) and gradient-echo pulse sequences are very relevant in MRI. A SE pulse is produced by pairs of radiofrequency (RF) pulses, whereas gradient-echo pulse is produced by a single radiofrequency pulse in conjunction with a gradient reversal (Figure 6).

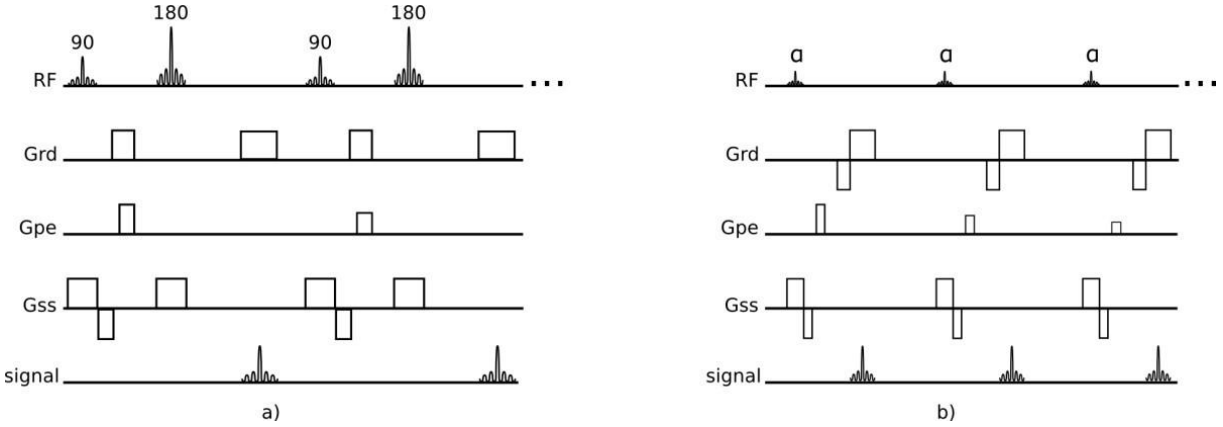

Figure 6 - Spin Echo pulse sequence (a) and Gradient -echo pulse sequence (b). There are 5 events that compose the pulse sequence: radio frequency pulses (RF), readout gradient axis (Grd), phase-encode gradient axis (Gpe), slice-selection gradient axis (Gss) and acquired echoes (signal).

1.3.1. Spin-Echo Sequences

Spin-Echo sequences offer a bigger ability in obtaining different contrasts depending on the choice of TE and TR. These different contrasts can be T1-weighted, T2-weighted or proton density-weighted. SE sequences refocus the excited signal with a 180° pulse (or pulses) and this makes the signal less vulnerable to off-resonance effects that can be caused by main field inhomogeneities or magnetic susceptibilities.

The main disadvantages of this type of sequences are their sensitivity to motion and flow and their limited temporal-resolution. There is also the option to shorten the SE sequences acquisition times and, in this situation, the SE pulse sequence becomes turbo SE, fast SE or rapid acquisition with relaxation enhancement. The acquisition times are shortened using a multi-echo approach in which multiple refocused echoes are acquired preceded by a single 90° excitation pulse (Figure 7). The reduction of acquisition time allows the acquisition of a whole image within a breath-hold, reducing the artifacts that could occur from breathing motion.

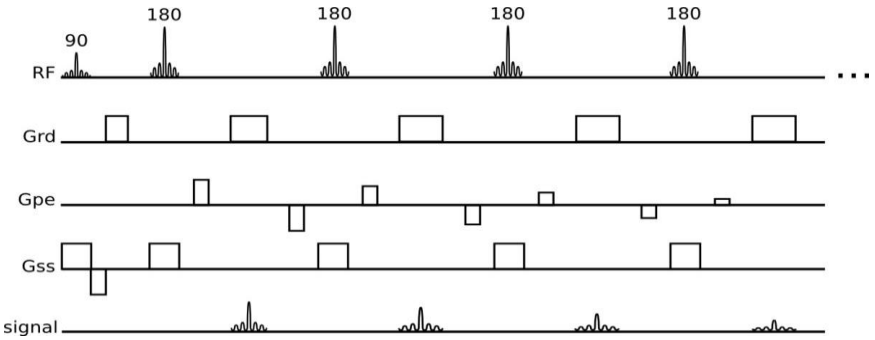

Figure 7 - Turbo Spin -Echo, Fast Spin -Echo or Rapid Acquisition with Relaxation Enhancement sequence.

1.3.2. Gradient-Echo Sequences

Unlike SE sequences, gradient-echo sequences do not have refocusing pulse. This makes the signal more susceptible to off-resonance effects, which makes this class of sequences generally T2* weighted instead of T2, thus because of the faster signal decay there is a need for shorter TE.

Gradient-Echo sequences allow faster image acquisition than SE sequences, which is an advantage for MRI characterization of the cardiac cycle. This rapid acquisition does not allow either the longitudinal or transverse magnetization to fully relax between successive radiofrequency pulses. The magnetization achieves an equilibrium state, known as steady state during the multiple excitations of the sequence. There are two strategies that can be employed to deal with the remaining magnetization at the end of each TR: the remaining transverse magnetization can be spoiled in Gradient-Recalled-Echo sequence (Figure 8a) or it can be refocused and reused as in the balanced steady–state free precession sequence (Figure 8b). Using this sequence is possible to obtain cine imaging. Cine sequences consist of a group of images at the same spatial location covering one full period of the cardiac cycle.

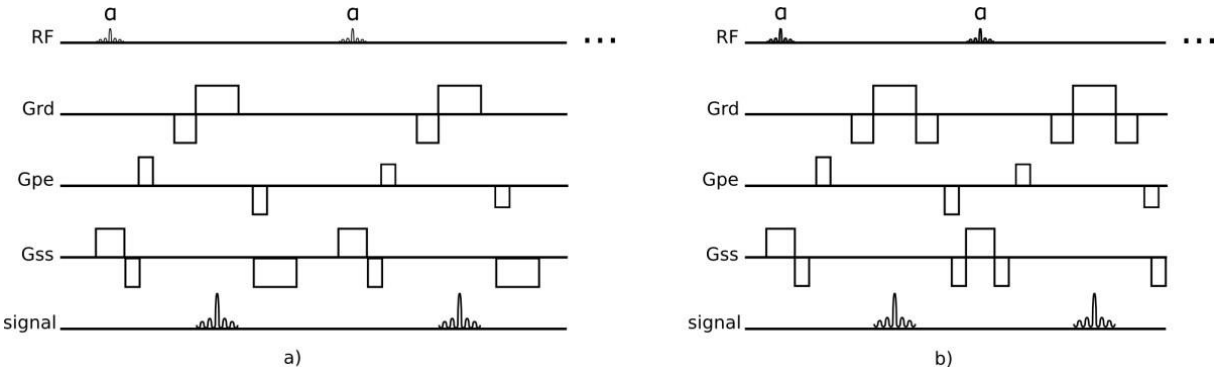

Figure 8 - Spoiled Gradient-Recalled Echo Sequence (a) and Balanced Steady-State Free Precession Sequence (b).

1.3.3. 4D Phase Contrast Imaging

Phase Contrast (PC) imaging allows quantitative blood velocity information. Combining this sequence with the ability of mapping the cardiac cycle via cine imaging to produce images

throughout the time, it is possible to visualize and quantify blood flow velocity within the heart or vascular regions of interest in 3D and over time (4D) (Figure 9).

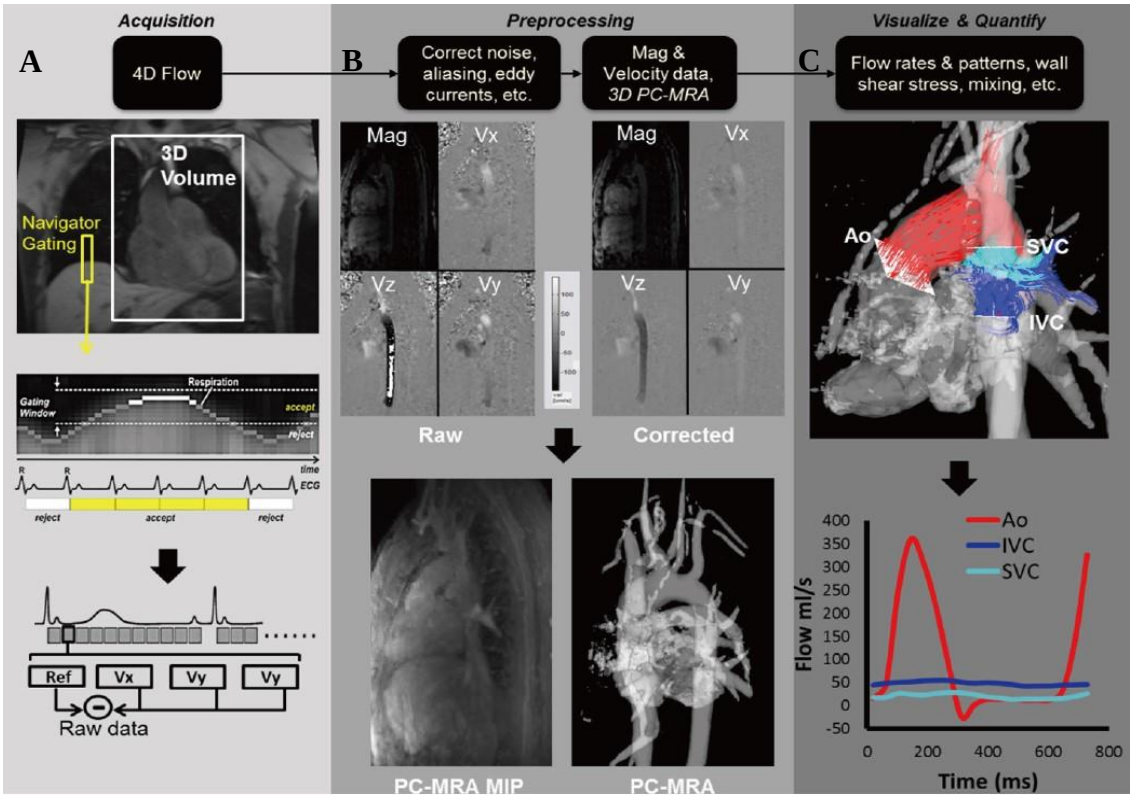

Figure 9 - Data acquisition and analysis workflow for 4D flow MRI. (A) 4D flow MRI data covering the whole heart (white rectangle) is acquired using ECG gating. 3D velocity-encoding is used to obtain velocity-sensitive phase images which are subtracted from areference image, in order to calculate blood flow velocities along all three spatial dimensions (Vx, Vy, Vz). (B) Data preprocessing corrects for errors due to noise, aliasing and eddy currents. Then the 3Dphase-contrast-MRI is calculated. (C) 3D Blood flow is visualized by emitting time resolved pathlines from analysis planes in the Aorta, Inferior Vena Cava and Superior Vena Cava. In addition, retrospective quantitative analysis can be used to derive flow -time curves at user selected regions of interest in the cardiovascular system [101].

The applications of gradient pulses induce phase shifts in moving protons that are directly proportional to their velocity along the direction of the gradient. For accurate quantification of this phase shift, a reference image is acquired separately to subtract phase shifts induced by other uncontrollable factors, such as magnetic field inhomogeneities. From repeating the acquisition for 3 orthogonal directions, it is possible to obtain phase maps which encode velocity (V_H, V_I, V_J) to a maximum velocity defined by the user (VENC). VENC stands for velocity encoding and should be chosen to enclose the highest velocities likely to be encountered within the vessel of interest. The VENC parameter adjusts the bipolar gradients. This means that, the maximum velocity selected corresponds to a 180° phase shift in the data. Thus, for each pixel, the measured phase depends on the velocity of the spins. Thus, stationary protons appear grey, spins that flow in the direction of the gradients appear brighter, and spins that move in the opposite direction appear darker. This is visible by an inverted signal where the intensity signal has a maximum brightness correspondent to phase shifts that overcome ±180°. Given this, the

velocity, **v**, within each voxel can be determined by the mean of the protons phase difference, **ΔΦ**, accrued during one time step (temporal resolution), using the formula:

$$\Delta\Phi = \gamma \Delta m v \tag{1.1}$$

where **γ** is the gyromagnetic ratio and **Δm** denotes the difference of the first moment of the gradient-time curve. On the other side, a too high VENC for the selected region will induce significant levels of noise.

The closer the VENC is to the maximum expected velocity (ideal VENC), the more precise is the measurement. If the VENC selected is lower than the velocity within the vessel, aliasing or phase wrapping occurs. However, a VENC setting of three times the ideal value (on low velocity regions) is considered to be an acceptable value [21]. There are clinical guidelines for VENC determination such as 100, 200, 400 cm/s for normal tricuspid valve, healthy aorta and tricuspid valve stenosis, respectively [22].

Sources of errors in PC-MRI acquisitions include inadequate VENC values, deviation of the imaging plane during data acquisition (e.g., cardiac, respiratory bad gating or patient motion), inadequate temporal or spatial resolution, and field inhomogeneity (e.g., susceptibility artefact from metallic implants). Therefore, depending on the structure of interest, PC-MRI parameters should be set in order to minimize potential sources of error [23].

1.3.4. Phase Wrapping

As described in the previous subsection, phase is a parameter of interest for the measurement and analysis of the blood flow. If the value of phase extends beyond 360 degrees or, in other words, if the dimensions of an object exceed the defined field-of-view, the redundant phase will be folded back into this range, leading to ambiguity in the final phase. This will induce an artifact in the image called phase wrap-around. The wrap-around artifact is generally recognized as a folding over of anatomic parts into the area of interest. (Figure 10) [24].

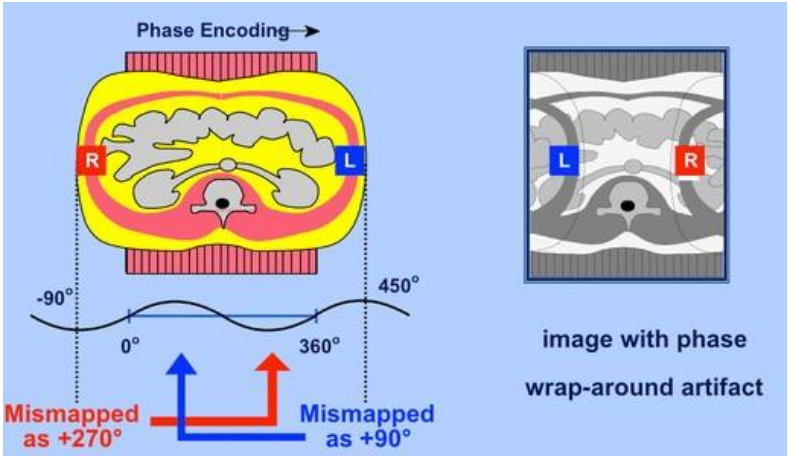

Figure 10 - Origin of the wrap -around artifact. Two regions (R and L) are both mismapped at different phases, and these redudant phases are foldedback into the range of acquisition.[100]

2. Fluid Mechanics applied to blood vessels

To develop a mathematical method to obtain absolute pressure gradients in both aorta and AV, it is necessary to understand their hemodynamic performance and the physical laws that govern their function.

2.1. Principle of Conservation of the mass

The principle of conservation of mass is a mass balance over a certain control volume. This volume can coincide with a section of an artery, with the LV or even with the surface of a blood cell. The boundaries of the control volume are usually chosen to give information regarding unknown flow rate, average velocity or surface area flow into or out of the volume [25].

The density of blood is constant, and since mass is the product of density and volume, mass conservation can be expressed as volume conservation for cardiovascular applications. The equation that expresses follows:

$$\frac{V_f - V_i}{t} = Q_{in} = Q_{out} \tag{2.1}$$

in which Q_{UV} is the total flow rate into the control volume, Q_{WXS} is the total flow rate out of the control volume, V_U is the size of the control volume at the beginning of the observation, and V_Y is the size of control volume after an observation time t. This equation is true for control volume that change with time, such as the volume of the LV. However, for most blood vessels, is possible to consider that the volume does not change with time. In these cases, the left side of equation 2.1. is zero, and conservation of the mass can be expressed as:

$$Q_{in} = Q_{out} \tag{2.2}$$

Flow rate in circular and nonbranching vessels can be decomposed into an average velocity $\bar{v}$ and a cross sectional area (CSA). In this case conservation of the mass can define unknown average velocities or CSAs into or out of the control volume:

$$\bar{v}_{in} A_{in} = \bar{v}_{out} A_{out} \tag{2.3}$$

2.2. Mechanical Energy and Bernoulli's equation

Mechanical energy can be described as the capability to accelerate a mass of material over a distance. There are three forms of mechanical energy per unit volume in the circulation: pressure, gravitational and kinetic energy. Even though pressure is the primary form of mechanical energy per unit volume in the healthy arterial circulation, in cases of diseased or venous circulations, gravity and kinetic energy play a significant role in the movement of flow [26].

Pressure (P) represents a force (F_p) per unit area. If this force is responsible for moving a mass (m) over a distance (d), it performs work, expending pressure energy ($E\_$). The area where the force acts on multiplied by the distance represents a volume (V):

$$P = \frac{E_P}{V} = \frac{F_P}{A} \tag{2.4}$$

A mass (m) accelerating due to gravity (g) creates a force (F_g). If this force moves the mass over a vertical distance (h), it too performs work and expends gravitational energy (E_g). The energy per unit volume is obtained by substituting density (ρ) for mass per unit volume:

$$\frac{E_g}{V} = \frac{F_g h}{V} = \frac{mgh}{V} = \rho g h \tag{2.5}$$

If a mass (m) is moving at a velocity (v), it contains kinetic energy, equivalent to half the product of mass and the square of the velocity of the mass:

$$\frac{E_k}{V} = \frac{\frac{1}{2}mv^2}{V} = \frac{1}{2}\rho v^2 \tag{2.6}$$

All the mechanical energy per unit volume forms can be freely converted from one to another without energy loss. Bernoulli's equation for steady flow relates the relative amounts of pressure, gravitational and kinetic energy per unit volume between two spatial locations along a path of a flow (locations 1 and 2, where 2 is downstream of location 1):

$$\frac{1}{2}\rho v_1^2 + \rho g h_1 + p_1 = \frac{1}{2}\rho v_2^2 + \rho g h_2 + p_2 \tag{2.7}$$

Bernoulli's equation for steady flow states the total mechanical energy per unit volume at locations 1 and 2 is the same but can exist in different forms. It shows that a decrease in pressure from location 1 to location 2 may be balanced from an increase in either fluid velocity or height without loss of energy. A pressure drop is therefore not mechanical energy loss if it is accompanied by increases in either gravitational or kinetic energy [26].

Two examples are illustrated in Figure 11. As a first example, blood enters the top of an inclined tube with a pressure of 100 mmHg and flows out at a pressure of 178 mmHg. The fluid moves against a pressure gradient from a point of low pressure (the beginning of the tube) to a point where the pressure is higher (end of the tube). However, the total fluid energy remains constant because the gravitational energy decreases is equal to the increase in pressure. This is what occurs in the arteries of a standing person (Figure 11A). As a second example, blood flows through a horizontal tube while the cross-sectional area increases 16 times. This results in a proportional decrease in fluid velocity. Again, the fluid moves against a pressure gradient, the pressure at the exit of the tube being 2.5 mm Hg greater than the pressure at the entrance to the tube. The total fluid energy remains the same because of the decrease in kinetic energy. This phenomenon is rarely observed in the human circulation because associated energy losses effectively mask the slight rise in pressure. (Figure 11B) [26].

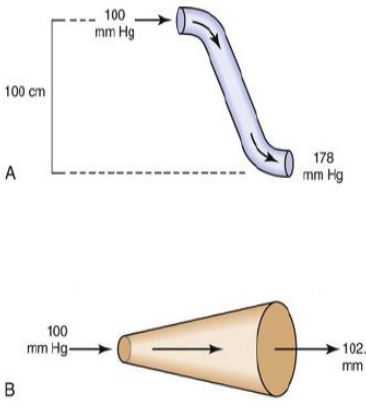

Figure 11 – **(A)** Effect of vertical height on pressure in a frictionless fluid flowing downhill. **(B)** Effect of increasing cross-sectional area on pressure in a frictionless fluid system. Adapted from [3].

To account for the effects of unsteady flow and mechanical energy loss, additional variables can be added to Bernoulli's equation for steady flow:

$$\frac{1}{2}\rho v_1^2 + \rho g h_1 + p_1 = \frac{1}{2}\rho v_2^2 + \rho g h_2 + p_2 + \int_1^2 \rho \frac{\partial v}{\partial t} \partial s + \Phi \quad (2.8)$$

where s represents the distance of the path between locations 1 and 2 and Φ represents loss of mechanical energy per unit volume. The two added terms represent the contribution of temporal acceleration of the fluid to the flow energy and the conversion of mechanical energy to heat, respectively, between locations 1 and 2 [26].

2.3. Poiseuille's law

The specifications of the Bernoulli equation are theoretical and non-possible to achieve in human circulation. Mechanical energy can be lost in the movement of blood or fluid from one point to another (and normally is converted to heat). Energy loss is related to the viscosity of blood and its inertia. In fluids, viscosity can be defined as the friction between adjoining layers of fluid. This friction is due to strong intermolecular attractions between fluid layers. Poiseuille's law describes the viscous energy losses occurring in an idealized situation [26].

$$P_1 - P_2 = \bar{V}\frac{8L\eta}{r^2} = Q\frac{8L\eta}{\pi r^4} \quad (2.9)$$

in which $P_q - P_F$ is the pressure drop between two points separated by the distance L, Q is the volume flow, and $\bar{V}$ is the mean flow velocity across a tube with an inside radius of r. From Equation 2.9 is possible to establish that energy losses are inversely proportional to the fourth power of the radius. Figure 12 illustrates the Poiseuille's Law in different cases. It shows that, until a certain degree of narrowing is reached, there is little effect on the pressure. Beyond that point, further reductions in diameter cause the pressure gradient to rise rapidly. Although increasing the flow rate shifts the curves to the left and linearly increases the pressure gradient at any given radius, these effects are much less marked than those caused by changes in radius.

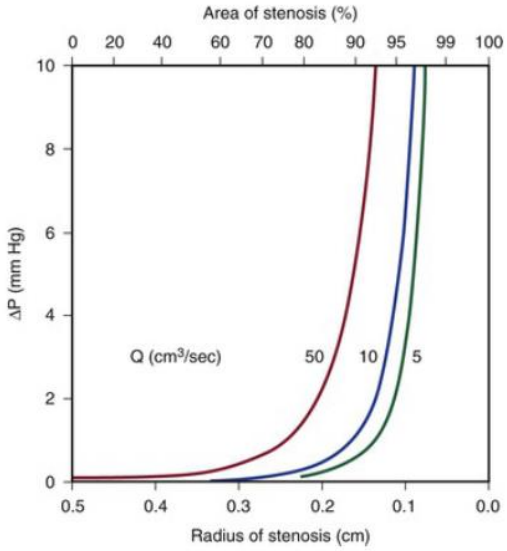

Figure 12 - Example curves derived from Poiseuille's Law. There are three curves of the pressure gradient behavior with the increase of area of stenosis for different volume flows: 50 cm^3/s (red), 10cm^3/s (blue) and 5 cm^3/s (green) [1].

2.4. Energy Losses associated with stenosis

Most of the abnormal energy losses in the arterial system result from stenosis or obstruction of the vascular lumen. In accordance with Poiseuille's law (Equation 3.9), the energy losses are inversely proportional to the fourth power of the radius at the stenosis and are directly proportional to the length of the stenosis. Therefore, the radius of a stenosis is much more significant than its length [26]. In addition, inertial energy losses are encountered at both the entrance to and the exit from a stenosis [27, 28]. The magnitude of these losses varies with the shape of the entrance and exit. The energy losses associated with asymmetrical stenosis exceed those associated with symmetrical stenosis, even when the lumen is compromised to the same extent [28, 29]. Although energy losses at the entrance can be appreciable, they are usually greater at the exit, where much of the excess kinetic energy resulting from the increased fluid velocity within the stenosis is dissipated in a turbulent jet.

Experimentally, appreciable changes in pressure and flow do not occur until the cross-sectional area of a vessel has been reduced by more than 75% [30]. The degree of narrowing at which pressure and flow begin to be affected has been called the "critical stenosis."

Energy losses across stenotic segments also depend on the velocity of blood flow (as shown in equation 3.8). Significant drops in pressure and flow occur with less severe narrowing in high-flow systems than in low-flow systems [31].

Precise attempts to relate pressure and flow restriction to percentage stenosis have been frustrated by the irregular geometry of arterial lesions and by the nonlinearities introduced by pulsatile blood flow. For practical purposes, any lesion that potentially decreases the arterial lumen by about 75% cross-sectional area or 50% diameter must be suspect, and its hemodynamic significance must be determined by objective physiologic tests.

The method proposed in this thesis attempts to calculate the peak-to-peak pressure drop using flow rate, velocities and relative pressure measurements obtained via MRI, in both patients of CoA and AvD. Both studies were approved by institutional research ethics committee following the ethical guidelines of the 1975 Declaration of Helsinki. Written consent was obtained from the participants and/or their guardians.

3. Materials

3.1. Catheterization

Routine catheterization procedures aiming to make a final treatment decision were performed under monitoring with a Philips Allura Xper FD 10/10 biplane angiography system (Philips Medical Systems, Best, The Netherlands), using contrast agent injection (Ultravist, Schering, Berlin, Germany). The pressure curves were recorded (Schwarzer Haemodynamic Analysing System, Heilsbronn, Germany) in two predefined locations via catheter pull back. Peak-to-peak pressure gradients across CoA and AvD were obtained from these pressure curves and used to validate MRI based pressure mapping.

3.2. Doppler Echocardiography

Diagnostic echocardiography was performed from the jugular fossa using a 3.5 MHz transducer interfaced with a Vivid E9 and processed with EchoPAC (GE Healthcare, Chicago, Il, USA). The continuous wave Doppler beam was aligned with the narrowing region to detect the maximum velocity *Vmax* through the CoA. The pressure gradient is obtained via the simplified Bernoulli equation:

$$\mathrm{dp} = 4(Vmax)^2 \qquad (4.1)$$

3.3. MRI equipment and protocol

MRI was conducted, before catheterization, in a 1.5 T magnetic resonance scanner (Achieva R 3.2.2.0, Philips Medical Systems, Best, the Netherlands) using a 5-element cardiac phased-array coil (Philips Medical Systems). Three directional blood flow velocities (v_x, v_y, v_z) were measured over the cardiac cycle using anisotropic k-space segmented 4 directions velocity encoded MRI (4DVEC-MRI) with electrocardiographic gating. The acquisition covered the full LV and the thoracic Aorta (ascending, arch and descending). Exemplary 4D-VEC-MRI scan parameters were: FOV feet-to-head 180 mm; anterior-to-posterior 200 to 230 mm (depending on size of the patient); rightto-left 90 to 105 mm (depending on number of slices and slice thickness); acquired voxel 2.5 × 2.5 × 2.5 mm; reconstruction matrix 128 × 128; reconstructed voxel 1.7 × 1.7 × 2.5 mm; flip angle of 5°; shortest TR and TE; nominal temporal resolution varying with heart rate for 25 cardiac phases; and velocity encoding 400 cm/s. Scan time varied between 8.5 and 14 min, depending on the chest size of the patient. 3D anatomy MRI was acquired at end-diastole. The typical scan parameters were: acquisition matrix 100x100; voxel size 1.2×1.2×2.0mm; repetition time 3.6ms; echo time 1.8ms. Acquisition duration was typically 2 min.

3.4. Post Processing Software

3.4.1. MevisFlow

Although non-invasive measurements of patient 4D hemodynamics have been facilitated by the innovation of MRI techniques, the high number of processing steps and data complexity mean that data analysis remains challenging. MevisFlow software (Fraunhofer MEVIS, Bremen, Germany) introduced new processing and visualization approaches for 4D PC-MRI data. Some

features included in the software are 3D flow visualization, velocity vector field quantification and color coding of local hemodynamic according to, for example, local velocity or pressure. In the context of this work, this program was used in both CoA and AvD studies to: perform semi-automatic watershed 3D segmentation of the lumen and create the mask of the aorta and AV region; determine the blood velocity and flow patterns in the mask; calculate and visualize the relative pressure maps. This is accomplished by using particle tracing based on the magnitude and three directional field images together with the previously segmented aorta.

3.4.2. GTFlow

GTFlow (GyroTools LLC, Winterthur, Switzerland) is a software that delivers all the necessary functionality for visualization, assessment and interpretation of multidimensional MRI phase-contrast flow datasets. In opposite to MevisFlow, it allows the creating of new visualization planes, perpendicular to the MRI sequences. This software was only used for the AvD study, to create a plane in the valve area and obtain the hemodynamic values in that region.

4. Non-Invasively Measurement of Absolute Gradient Pressure via Cardiac Magnetic Resonance in Patients with Coarctation of the Aorta

This study aims to develop a MRI-based time-shift corrected pressure mapping (TCPM) to assess pressure gradients and to validate it against peak-to-peak pressure differences obtained from invasive heart catheterization. We further aimed to compare this method against other commonly used noninvasive measurements based on cuff pressures and Doppler echocardiography.

4.1. State of the art

The diagnosis of CoA is usually based on clinical examination, and all the investigations were and are directed at defining its size and nature, using a less invasive technique, to allow a correct surgical approach. Doppler Echocardiography and cardiac catheterization are two of the methods most used to diagnose and characterized CoA.

The gold-standard for the measurement of pressure gradients in the aorta is the cardiac catheterization. Cardiac catheterization is a clinical procedure used to diagnose heart conditions. A long and thin tube (catheter) with a specific ending, depending on the aim of the intervention, is inserted at the groin and is passed through the blood vessels, until it reaches the aorta. The catheterization can be used to measure several blood functional and structural parameters as blood pressures [31, 32], cardiac output [33] or myocardial metabolism [34].

Doppler echocardiography is a non-invasive method that can be an alternative for cardiac catheterization. From this method is possible to detect acceleration and turbulence within the region of the narrowing, and determine the CoA severity with the pressure gradient analysis. Per Hudson et al., Doppler echocardiography techniques might be expected to be able to confirm the presence and site of the obstruction and measure the pressure difference across it. However, these techniques underestimate the pressure gradient in some patients because of misalignment with the direction of flow or because of the small size of the orifice [35].

In 1996, J. L. Oshinski et al. evaluated the accuracy of Doppler ultrasound in measuring the pressure gradients in patients with CoA. Although acquiring consistent results is very ambitious because of the difficulty of obtaining a clear acoustic window from lung tissue, an advantage of this method is that it can be used to estimate the pressure gradient across CoA. These estimates were obtained using the simplified Bernoulli equation, which assumes certain points that cannot be easily corrected:

a) The velocity proximal to the stenosis is negligible, and this assumption is only reasonable for severe stenosis.

b) For severe stenosis, there are highs levels of turbulence in the flow field near the throat of the stenosis. This turbulence may cause an irreversible pressure loss and the simplified Bernoulli equation will not account for this pressure loss and hence underestimate the stenosis severity [36].

c) The shape of the stenosis is a factor that can cause errors in the pressure gradient estimates using the simplified Bernoulli equation. The shape of the stenosis severity will also affect the value of loss coefficient [37].

This study also suggested that MRI could be used as a complete diagnostic tool for accurate evaluation of CoA, by determining the narrowing location and severity and by estimating accurately pressure gradients. Unlike echocardiography, MRI has the ability to image in any desired plane and with a nearly unrestricted FOV, allowing a great flexibility to evaluate abnormal cardiac and extra cardiac structures [38].

Several studies [39] already determined that MRI is superior to ultrasound in determining the location of CoA and compares well in estimating CoA severity. More recent studies [40-42] have

concluded that is possible to predict the non-invasive pressure gradient with good agreement using MRI, however no efforts have been made or have resulted in acquiring the absolute pressure noninvasively.

4.2. Methods

A total of n=27 patients (n=16 male, n=11 female, age range 4 to 52 years, mean age 20±15 years), that had clinical indications for cardiac catheterization based on Echo, arterial hypertension and/or MRI, were included.

4.2.1. MRI – Data Processing

The PC- magnetic resonance angiography (PC-MRI) was computed from original 4D-VECMRI images in MevisFlow (Fraunhofer MEVIS, Bremen, Germany) allowing the distinction between blood and static tissue from the phase differences [43, 44]. To segment the aorta, watershed 3D segmentation of the lumen, based on anatomical high resolution 3D Whole Heart, was performed using the software ZibAmira (Zuse Institute Berlin, Berlin, Germany) [45]. The masks of the aortas of each patient are present in Annex I.

Subsequently, the segmentation previously made was selected as the aorta, from which the relative pressure maps were generated and blood flow data (net flow, pressure, velocity and area in each ROI). The relative pressure maps of each patients are present in Annex II. A vessel size reduction by 5% was applied in order to avoid the numerical inconsistencies close to the vessel wall, that can normally occur when using the Pressure Poison Equation [46]. This vessel reduction was not critical because it was not within the objective of this study to analyze the pressure condition near the vessel wall.

4.2.2. MRI Pressure Gradients Processing

Diagnostic echocardiographic examination was done in clinical setting using 3.5 MHz transducer interfaced with a Vingmed system V (GE Vingmed Ultrasound AS, Horten, Norway). The continuous wave Doppler beam was aligned with the narrowing region to detect the maximum velocity *Vmax* through the CoA. The pressure gradient is obtained via the simplified Bernoulli equation (Equation 4.1).

The aorta segmentation was based on anatomical higher resolution of the 3D Whole Heart sequence.

To analyze aortic velocity fields, 4D-VENC MRI data was processed in MevisFlow (Fraunhofer MEVIS, Bremen, Germany): Initial anti-aliasing was applied in the presence of phase wrapping [47]. Then, the 3D Whole Heart based segmentation was registered to 4DVENC MRI data. After registration, the anatomical segmentation was used as 3D mask for further Pressure Mapping procedure. From the 3D mask of the aorta, the hemodynamic data (net flow, pressure, velocity and area in each ROI) was acquired. To generate the relative pressure maps, Pressure Poisson equation is solved with inhomogeneous Neumann boundary condition using the finite-element method, as suggested by Meier *et al.*[48]:

$$-\Delta p = \nabla.(\rho u.\nabla u - \mu\nabla^2 u - \rho g) \tag{4.2}$$

A mask size reduction of 5% was applied in order to avoid the numerical inconsistencies close to the vessel wall, which can occur when using the Pressure Poison Equation.[49, 50] From the relative pressure maps, the pressure difference is obtained at the instant when the flow rate is maximal in ascending aorta. The equation 4.2 does not consider the inertial term that is the first term of the Navier-Stokes equation for the momentum conservation (equation 4.3):

$$\rho\left(\frac{\partial u}{\partial t} + u.\nabla u\right) = -\nabla p + \nabla.\left(\mu(\nabla u + (\nabla u)^T) - \frac{2}{3}\mu(\nabla.u)I\right) + F \qquad (4.3)$$

where u is the velocity, p is the pressure, ρ is the blood flow density (ρ = 1060 kg/m^3), μ is the dynamic viscosity and F the external forces applied to the fluid [47, 50].

The Windkessel function of the distensible aorta accounts for the shape of the arterial blood pressure waveform. The walls of large elastic arteries, such as the aorta, contain elastic fibers. These arteries distend when the blood pressure rises during systole and recoil when the pressure drop decreases during diastole. Since the rate of blood entering elastic arteries exceeds the amount of blood leaving them, due to the peripheral resistance, there is a net storage of blood during systole which discharges during diastole. The Windkessel effect can be illustrated as shown in Figure 13.

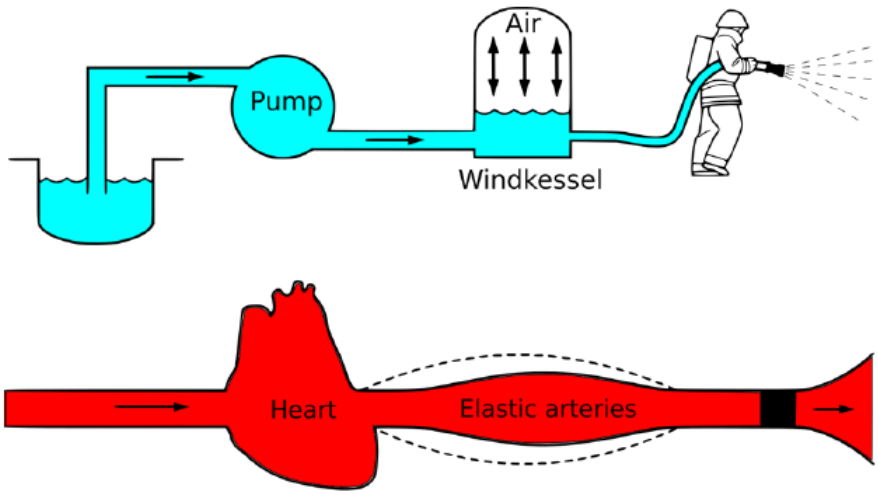

Figure 13 – The Windkessel effect can be compared to the air chamber used in fire engines. The Windkessel effect helps in alleviate the fluctuation in blood pressure over the cardiac cycle and assists in the maintenance of organ perfusion during diastole when cardiac ejection ceases.

However, the Windkessel function of the distensible aorta causes a pulse pressure propagation with a pulse wave velocity [51]. Thus, a time-shift between both, pressure and volume flow curves in ascending and descending aorta is observed. Consequently, as the fluid acceleration/deceleration in the ascending aorta is zero, the fluid downstream is accelerating or decelerating causing additional positive or negative pressure gradient. To take this into account, we propose a correction of the pressure gradient calculated by equation 4.2 by using a follow simplified approach:

$$dp_{corr} = -\rho\left(\frac{\Delta u}{\Delta t}\right)dx \qquad (4.4)$$

where dx is the distance between predefined locations in the ascending and the descending aorta, Δt is the time shift between peak flow rates in the ascending and the descending aorta and the Δu is the

change of the mean velocity at the descending aorta site during the time shift (period between peak flow at the ascending and peak flow at the descending aorta). The synthesis of the proposed method is shown in Figure 14.

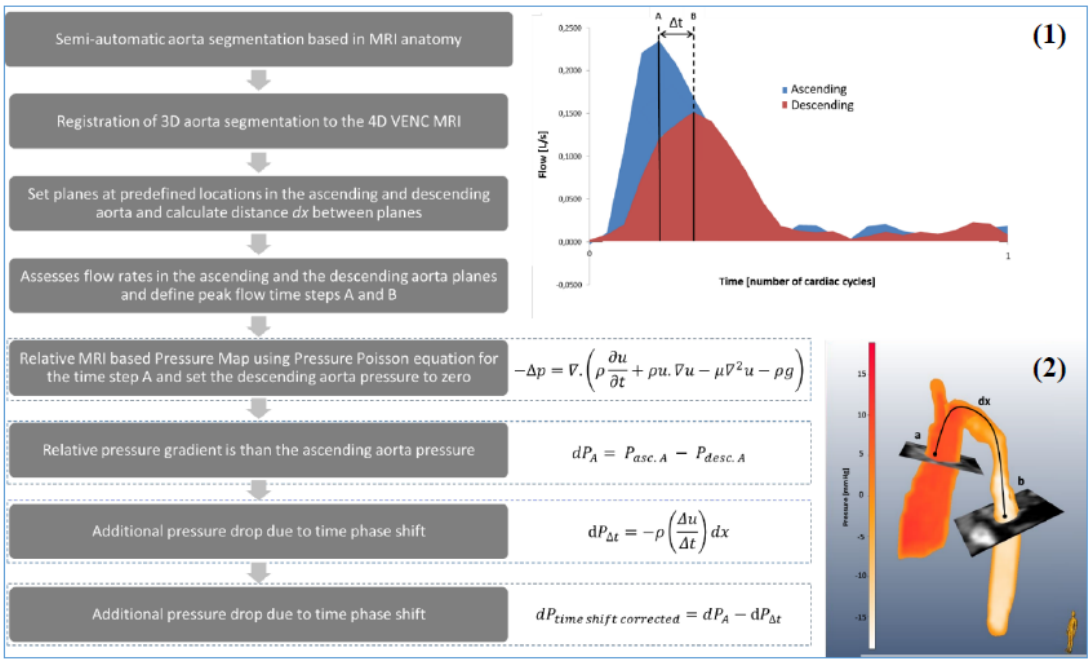

Figure 14 - Block diagram that illustrates the method follow and summarizes the equations used (1) Flow distribution in the ascending (blue) and descending (red) aorta. A and B are the time steps in which there is a peak flow in the ascending and descending aorta, respectively. (2) Relative pressure distribution / field / map of the aorta during systole. There are two planes, one in the ascending aorta and other in the descending aorta. dx is the distance between two planes.

To calculate the TCPM, further requirements must be considered. First, the ROIs must be cross sectional to the vessel and defined in ascending and descending aorta according measurement sites during catheterization procedure. The ROI in the ascending aorta is placed in the pulmonary trunk plane, whereas the ROI in the descending aorta is placed in the AV plane. The velocity vector field and pressure map must be continuous over the 3D mask.

4.2.3. Statistical analysis

The analysis of the data was performed with SPSS version 21 (IBM Corporation, Armonk, USA). Data is expressed as mean ± standard deviation (SD). Effects have been considered significant at $p < 0.05$. The Pearson correlation coefficients and linear regression have been determined. In addition, a two-one-sided test (TOST) procedure was used to test equivalency [57]. In this procedure, it is assumed that the population means differ – Null hypothesis – and the goal is to prove the population means equivalency – Alternative hypothesis.

To have an acceptable statistical power of 80%, a minimal sample size of 7 patients was necessary to compare both catheter and MRI measurements. The effect size was calculated based on SD of pressure gradients measured with a catheter (4.8 mmHg). The power test was performed for the T-test (differences between two dependent means − matched pairs). The power analysis was performed using G*Power 3.1.9 (Franz Faul, Kiel University, Kiel, Germany) [53].

4.3. Results

Initially there were 27 patients under analysis. In the beginning of our procedure, we had to eliminate 6 patients. The causes for each elimination, the patient characteristics, hemodynamic baseline measurements and MRI measurements are given in Table 3.

Per the power test, the sample size necessary to compare catheter and MRI measurements is 7 patients, which is much lower than the number of patients considered (n=21).

The TOST procedure indicated a $p<0.05$, thus the null hypothesis - the population means differ – is rejected, and the two populations can be considered practically equivalent.

Table 3 - Patients characteristics and values of absolute and relative pressure gradients obtained via catheter and MRI.

Patient	Sex	Age	RR Right Arm Pressure [mmHg]	Percentage of flow through the narrowing (%)	Absolute Pressure Gradient (Catheter) [mmHg]	Absolute Pressure gradient (MRI) [mmHg]	Relative Pressure gradient (MRI) [mmHg]	Relative Pressure Gradient (Doppler) [mmHg]
1	M	6	127/72	44.15	19.80	19.27	24.73	47.00
2	M	10	144/55	48.91	30.44	34.49	46.4	57.00
3	F	7	122/67	65.21	18.85	20.16	24.57	56.00
4	M	17	134/53	48.03	17.02	18.73	29.48	10.00
5	M	16	158/81	43.50	19.53	21.37	24.89	72.00
6	M	12	118/50	41.93	25.27	31.37	27.75	24.00
7	M	18	140/62	17.23	30.53	(1)		
8	M	4	145/79	26.18	31.20	(1)		
9	M	7	137/80	17.44	45.00	(1)		
10	F	24	132/70	43.97	28.00	20.25	26.53	49.00
11	M	20	140/60	58.85	30.80	56.79	58.29	30.80
12	F	40	110/65	45.30	27.33	11.96	15.32	27.33
13	M	19	124/81	40.28	21.00	27.45	31.86	43.60
14	F	29	152/85	50.03	18.25	44.50	49.37	39.10
15	M	52	151/76	42.34	15.00	19.55	23.21	24.19
16	M	15	99/60	17.70	17.70	14.97	18.75	18.00
17	M	17	175/105	56.85	21.33	29.31	31.84	41.55
18	F	46	182/78	55.23	17.10	28.86	31.83	43.60
19	F	14	154/72	57.69	15.33	(2)		
20	F	16	131/62	59.37	40.89	42.75	24.69	30.59
21	M	11	160/95	45.98	18.00	(2)		
22	F	31	190/109	62.48	24.66	29.42	13.44	32.68
23	F	61	168/78	59.73	17.25	23.05	21.49	25.47
24	F	22	148/94	50.57	16.00	21.90	23.85	27.58
25	F	14	160/94	59.00	22.00	22.77	40.03	60.50
26	M	15	121/88	84.01	32.00	31.16	15.11	56.97
27	M	42	148/77	50.23	20.30	(2)		
Mean Value ± Standard Deviation	-	21±14	-	47.85±15.21	22.86±6.64	25.47±6.68	28.73±11.49	38.90±15.89

(1) Patient eliminated due to low percentage of flow through the narrowing (less than 30%). (2) Patient eliminated because the aorta is not entirely inserted in the field of view of the acquired image.

From the Bland-Altman approach is possible to verify the measurements from catheterization (22.86±6.64 mmHg) and MRI (25.47±6.68 mmHg), have a good agreement. The bias (mean of differences) is -2.59 mmHg and the limit of agreement (double of the standard deviation) is ±4.74 mmHg (Figure 15). This approach also shows that Doppler Echocardiography (27.15±11.43 mmHg) overestimates the catheterization measurements. The bias is -19.25 mmHg and the limit of agreement is ±30.16 mmHg. The linear correlation equation between catheterization and TCPM measurements is $TCPM = 0.94\ Catheterization + 3.93$ and the linear equation between catheterization and Doppler echocardiography is $Doppler_{\text{echocardiography}} = 0.66\ Catheterization + 23.82$.

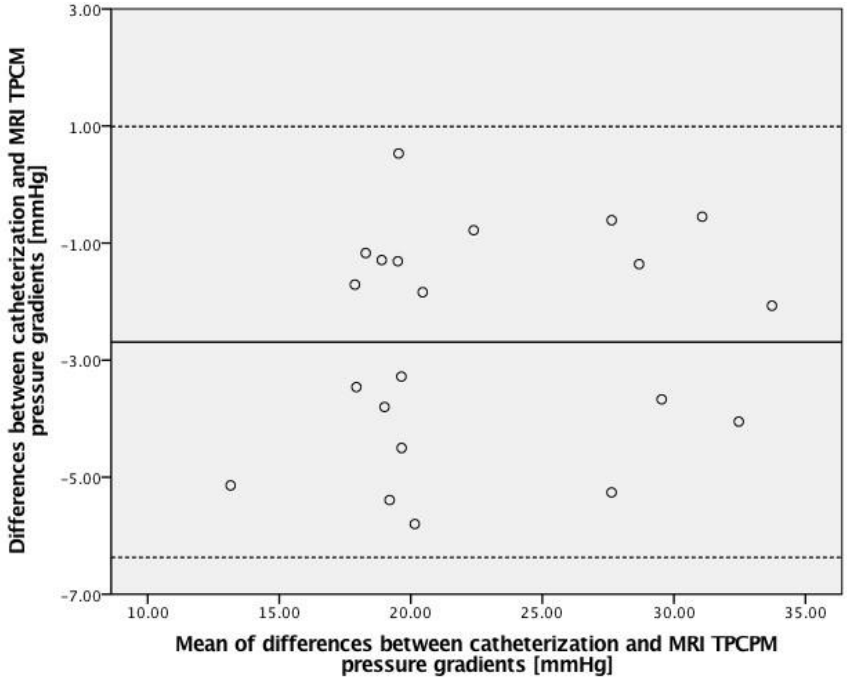

Figure 15 - Bland Altman analysis to compare catheterization and MRI TCPM. The bias is -2.59 mmHg and the limit is ±4.74 mmHg.

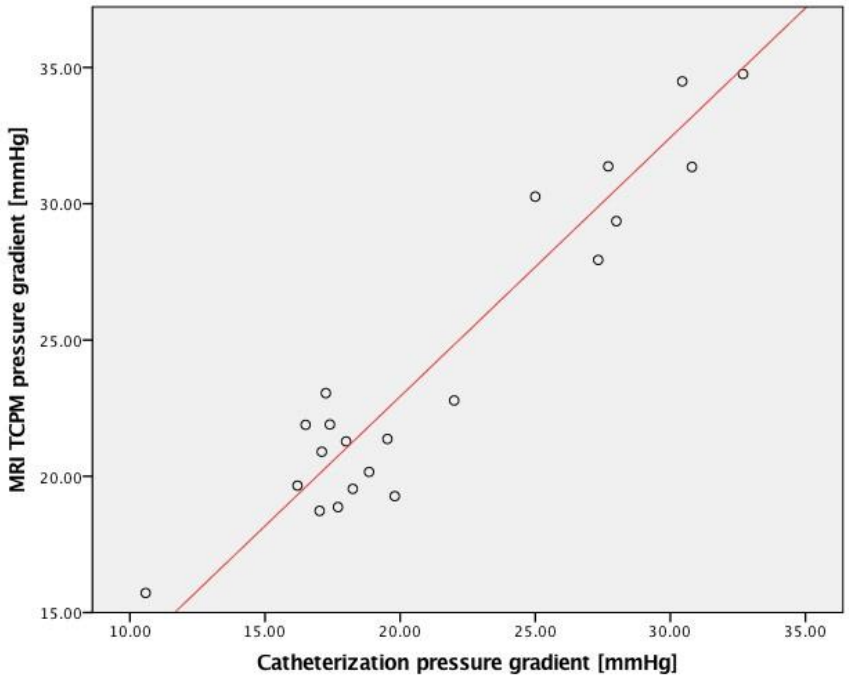

Figure 16 - Scatterplot of the measurements from catheterization and MRI in mmHg. The red line is the trend line of the linear correlation between the two methods. The correlation coefficient between both absolute measures (catheter and MRI) is 0.88. The correlation equation is $\boldsymbol{CMR = 0.94\ Catheterization + 3.93}$

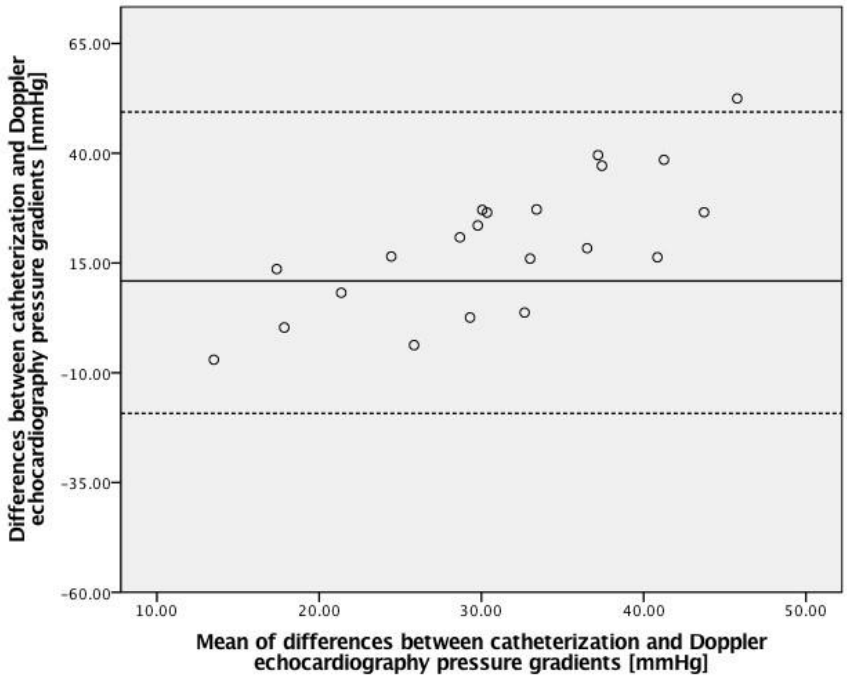

Figure 17 - Bland Altman analysis to compare catheterization and Doppler Echocardiography measurements. The bias is -19.25 mmHg and the limit is ±30.16 mmHg.

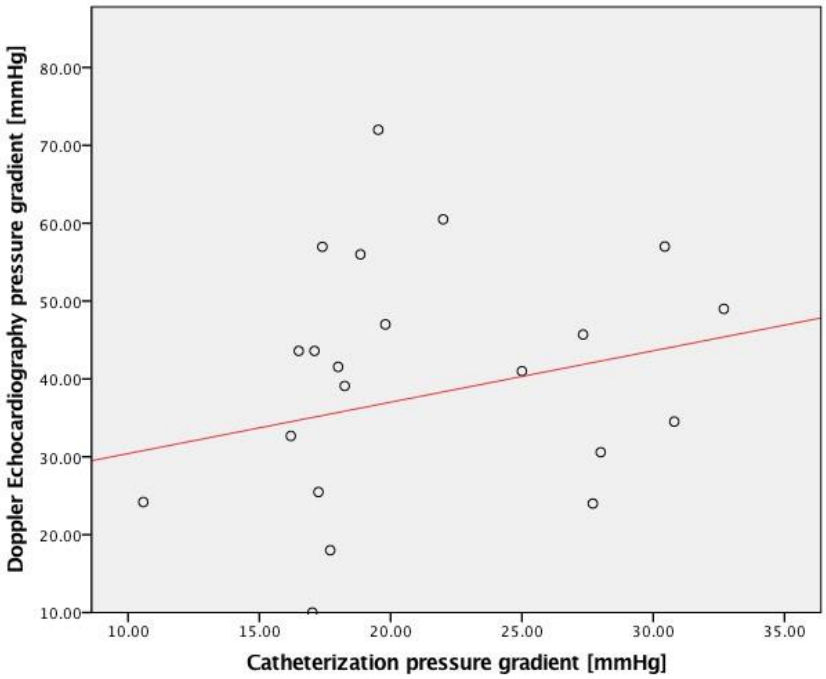

Figure 18 - Scatterplot of the measurements from catheterization and MRI in mmHg. The red line is the trend line of the linear correlation between the two methods. The correlation coefficient between both absolute measures (catheter and MRI) is 0.07. The correlation equation is $\boldsymbol{CMR = 0.66\,Catheterization + 23.82}$

4.4. Discussion

The study presents a non-invasive MRI based method for TCPM. Measurements were performed on a group of patients with pressure gradients (21.34 ± 5.84 mmHg) in a typical clinical setting. The results show a good agreement between time-shift corrected MRI pressure maps and catheter derived peak-to-peak pressure gradients in CoA.

The ACC and AHA guidelines recommend intervention for CoA or re-CoA in the presence of arterial hypertension and if the peak-to-peak CoA pressure gradient exceeds 20 mmHg. If the pressure gradient is lower than 20 mmHg, but there is anatomic imaging evidence of significant CoA with radiological evidence of significant flow, intervention is also suggested. These guidelines focus the decision making in the peak-to-peak pressure gradients, which in clinical practice can only be measured by catheterization, an invasive method. The ESC guidelines recommend treatment in patients with upper limp hypertension (>140/90 mmHg) and non-invasive pressure gradients higher than 20 mmHg. Intervention is further indicated when CoA narrowing is severe with a reduction of over 50% of the vessel diameter in hypertensive patients, regardless of pressure gradient [54].

These guidelines point out the medical need for a non-invasive and an accurate method to measure pressure gradients across CoA. However, currently available tools are not always reliable., RR method is established as a valid method to measure arterial hypertension, RR measurements of pressure differences between peripheral arteries are affected by anatomic variation, pulse wave velocities and measurement set-up (e.g. cuff-size). Doppler is widely accessible and the first-choice method for diagnostic workup of patients with CoA. Doppler pressure gradient is obtained from simplified Bernoulli equation. This method can lead to pressure gradient overestimation, due to

increased arterial stiffness or underestimation in complex anatomy cases, due to FOV limitations [55]. Both statements agree with our results.

When compared to Doppler Echocardiography, MRI has the advantage of allowing the visualization of the anatomy of aorta and CoA, that can be difficult to assess by Echocardiography. Severe cases, with a vessel diameter reduction of over 50%, can be reliably detected. More recently, MRI-derived methods that allow the computation of 3D pressure maps relative to a reference location at all time-points were proposed [56]. Nonetheless, the relative pressure maps do not take into consideration the peak pressure time-shift along the aorta. If the time-shift, due to the Windkessel function, is neglected, the pressure variation that occurs in this interval is not weighed. Therefore, systematic errors in pressure gradient acquisition are induced and relative pressure maps tend to underestimate the pressure gradient across CoA. Which is also in conformity with our results [57].

The study of Riesenkampff *et al.* proposed a method that allows the acquisition of peak-to-peak CoA pressure gradients based on manual adjustment of peak pressures. This method improved the outcome of pressure gradients accessed via MRI, by introducing the time-shift correction to relative pressure maps. However, it is very inconvenient because it required calibration of catheterization pressure curves with RR upper limb absolute pressures at several aorta locations.

Our method allows non-invasive measurement of time-shift corrected pressure gradients in CoA patients, using the relative pressure gradient and pressure variation over time in the ascending and descending aorta. Several aspects have to be taken into account, in order to assure the accuracy of the method. The ascending and descending ROIs must be cross-sectional to the aorta, to obtain proper velocities, mean value, flow and relative pressures [17, 20, 21]. Since net flow is accepted as the most solid hemodynamic indicator of the aortic pulse wave, the maximal flow rate time points in ascending and descending aorta were considered as markers for the time-shift along the aorta [58].

Concerning MRI data processing, we applied the Pressure Poisson equation with inhomogeneous Neumann boundary conditions to generate the 3D relative pressure maps. Numerical inconsistencies can occur when using Pressure Poisson equation. To avoid such, there is a vessel size reduction of 5%. The vessel size reduction is not critical, since it is not the objective of this study to analyze the pressure conditions near the vessel wall [59]. The pressure maps based methods are dependent on the good quality of the 4D VEC MRI images. The quality can be affected by several conditions. Stents might induce phase shifts and radio frequency shielding. In the presence of severe narrowing, the percentage of blood that flows to the lower body via the collateral arteries is more significant. Since, these vessels are not included in the segmentation, due to limited FOV it is not possible to assess the impact of the collateral flow in pressure gradient measurements. Such cases should be further investigated.

The patients analyzed have moderate CoA under typical clinical setting conditions. Thus, the considered cohort of patients represents the borderline cases for CoA intervention. DopplerEchocardiography overestimated gradients in nearly all patients. For some patients, RR pressure did show large variability between left and right leg and/or higher pressure in the legs, when compared to the arms, which might indicate wrong cuff size, or further vascular complications. Additionally, arm-leg gradient can underestimate CoA pressure gradient in the presence of developed collaterals. Arterial hypertension was present in 52.4% of the cases [60, 61]. Even though, all the patients had catheterization indication, n=5 were neither hypertensive nor had a pressure gradient exceeding 20 mmHg. These cases reflect the need for an improved diagnostic workup, particularly for borderline conditions, to avoid invasive procedures.

4.5. Limitations and Future Work

The defined anatomic positions could be slightly different between catheter and MRI based measurements, and this could lead to bigger differences between both methods.

If the 4D-Flow sequence does not have the whole aorta in its FOV, the algorithm will not account all the blood flow and the estimation of the absolute gradient of pressure will be incorrect.

The centerline, one of the visualization mode options that MevisFlow offers and that display the pressure along the centerline for a specific time point, must be continuous. If it presents discontinuities, the mask should be further analyzed to assure there are not any holes.

In patients with a CoA stenosis radius smaller than 2-voxel dimension, the signal to noise ratio is too high and the spatial resolution of the acquisition is insufficient. The lack of spatial resolution is further enhanced by the pressure maps computation, that subtract one voxel in each direction from the original 4D flow vector fields, due to boundary conditions [62].

MRI and catheterization do not occur at the same time. However, the time interval between exams was minimized to 1 day median. The 4D VENC MRI spatial resolution might be a limitation in patients with severe narrowing. If stenotic radius is smaller than 2-voxel dimension, the signal to noise ratio is high and the spatial resolution of the acquisition in insufficient [5]. However, this patient cohort was not in the scope of our study.

Patients had conscious sedation during catheterization, which affects hemodynamics, while there was no sedation during MRI. These different acquisition conditions may justify the offset of TCPM pressure gradients when compared with catheterization peak-to-peak pressure gradients.

5. Measurement of Valve Pressure Gradients and Severity Assessment in AvD

The second objective of the present thesis aims to measure the TCPM in the AV, in patients with AvD. Three methods for assessing pressure gradients across the valve were compared: the one developed and described in sub chapter 5.2.2., Bernoulli method and Gorlin Area method.

5.1. State of the Art

The definition of AvD, how to characterize and how to diagnose each disease is present in Section 2.2.2.

The flow through the AV is pulsatile in nature, meaning it has periodic variations, and it depends directly on multiple factors, including LV systolic and diastolic functions, aortic pressure, LV geometry, among others. When ventricular pressure exceeds aortic pressure during ventricular systole, the AV leaflets open to allow flow through the valve. The outflow rate across the valve increases until peak systole, beyond which it starts to decrease. Pressure gradient over the valve varies with time, in the cardiac cycle. In AS, the flow rate behavior over time is changed and could allow the improved disease diagnosis.

Flow through a stenotic AV is well approximated to flow through a convergent orifice (Figure 17). The narrowed AV orifice and restricted leaflet opening create a hemodynamic imbalance, causing blood's acceleration of blood through the valve. The area formed by the free edges of the AV leaflets is known as the geometric orifice area (GOA) of the valve, whereas the area of the flow jet at the *vena contracta* (VC) is known as the effective orifice area (EOA). The pressure difference between the LVOT and EOA is referred to as Δ*P*max [62].

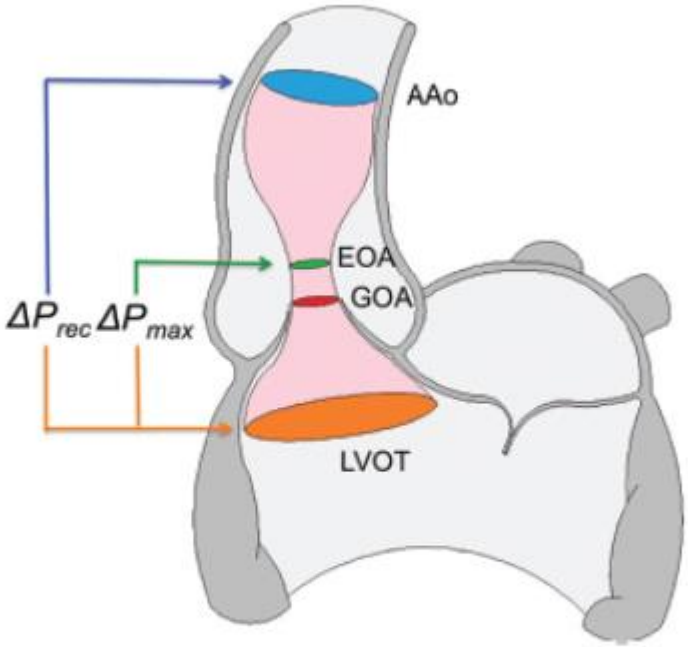

Figure 17 - Flow through a stenotic aortic valve. AAo indicates ascending aorta; EOA, effective orifice area; GOA, geometric orifice area; LVOT, left ventricular outflow tract; VC, vena contracta; VTI, velocity time integral [26].

The Gorlin Equation establish a relationship between GOA and ΔP*:*

$$GOA = \frac{Q}{c_c c_v \sqrt{2g\Delta P}} \tag{5.1}$$

where Q is flow through the AV, c is the contraction coefficient, c_p is the velocity coefficient, g is the gravity acceleration and ΔP is the pressure gradient. Simplifying equation 6.1 using the assumptions c = 0.85 and c_p = 1, the equation for the pressure gradient calculation is equation 5.2 [64, 65].

$$\Delta P = \left(\frac{Q}{44{,}3GOA}\right)^2 \tag{5.2}$$

5.1.1. Doppler Echocardiography

From Doppler echocardiography, the estimation of the diastolic pressure gradient is derived from the velocity flow curve through the AV, using the simplified Bernoulli equation:

$$\Delta P = 4v^2 \tag{5.3}$$

It has been already shown that this estimation is reasonable by the good correlation with invasive measurements using catheterization [63].

Doppler gradient is assessed using the apical window because it allows parallel alignment of the ultrasound beam and aortic inflow. The ultrasound Doppler beam should be oriented to minimize the intercept angle with aortic flow and to avoid underestimation of velocities. Color Doppler is useful to identify diastolic aortic jets that may be encountered in cases of severe deformity. In these cases, the Doppler beam is guided by the highest flow velocity zone identified by color Doppler.

To obtained well-defined and helpful contours of the flow, beam orientation and a good acoustic window are needed. Maximal and mean AV gradients are calculated by integrated software using the trace of the Doppler diastolic AV flow waveforms on the display screen. Maximal gradient is of little interest as it derives from peak AV velocity, which is influenced by left atrial compliance and LV diastolic function. [64] Both maximal and mean gradient are relevant hemodynamic findings and are useful parameters for the diagnosis of the disease. However, both of these parameters tend to overestimate the absolute pressure gradients [65].

In patients with atrial fibrillation, mean gradient should be calculated as the average of five cycles with the least variation of R–R intervals and as close as possible to normal heart rate [66].

AV mean gradient, although reliably assessed by Doppler, is not the best marker of the severity of AS since it is dependent on the aortic valve area (AVA), which is not easily measured and can have different values for different technicians measuring it, as well as a number of other factors that influence transmittal flow rate, the most important being heart rate, cardiac output, among others.[19] However, the consistency between mean gradient and other echocardiographic findings is needed for better decision-making, in particular in patients with poor quality of other variables or when such variables may be affected by additional conditions [i.e. pressure half-time (T1/2) in the presence of LV diastolic dysfunction] [67]. Pressure halftime is the time needed for the peak transvalvular pressure gradient to fall to its half value, in milliseconds.

5.1.2. Cardiac Catheterization

Typically, the pressure gradient is measured between the left ventricular outflow tract (LVOT) and the ascending aorta (AAo) by using double-lumen fluid-filled catheters for simultaneous LV and aortic pressure measurements. When artifacts extensively degrade the quality of the data or when additional precision is needed for the intended research, micromanometer-tipped catheters may be considered. CO is assessed in the cardiac catheterization laboratory by 2 principal methods: Fick and thermodilution [68]. The Fick method relies on obtaining arterial and mixed venous saturations, hemoglobin level, and oxygen consumption. The thermodilution method relies on injecting cold or room-temperature saline and measuring the change in temperature as this passes from the injection port to the thermistor on the Swan-Ganz catheter.

Once the pressure gradient and CO are obtained, the Gorlin equation is used to calculate the EOA.[72] However, this area differs from the corresponding echocardiographic measurement owing to the difficulty in precisely positioning the aortic side catheter at the VC of the flow jet. VC of the flow is the point in a fluid stream where the diameter of the stream reaches its minimum. In this point the fluid velocity is maximum. Despite the potential for inaccuracies, it is recommended that the operator perform a quick on-the-fly calculation of EOA by using the simplified Hakki equation (Equation 5.4) [69].

$$Aortic\ Valve\ area\ (cm^2) = \frac{Cardiac\ Output\ (\frac{litre}{min})}{\sqrt{Peak\ to\ Peak\ Gradient\ (mmHg)}} \tag{5.4}$$

5.1.3. Computed Tomography

Computed tomography (CT) is the method which provides the highest resolution of the AV, especially in cases of calcific AS [70]. Although cardiac CT was initially used to detect and quantify calcification in the coronary arteries, its applicability to assess AV calcification was also demonstrated [71].

Currently, multidetector CT scanner are most normally used because of their economic cost and both spatial and temporal superior resolution, when compared to angiography. In CT scans the calcific deposits show bright regions within the image, and the AvD can be characterized using the Agatston method. The metric of interest is the calcium score and it is obtained by multiplying the calcification area by an attenuation coefficient based on the peak attenuation in the region. The calcium score is expressed in Agatston Units (AU) [72].

A recent study showed that a calcium score <700 AU excluded severe AS, whereas a score >2000 AU suggested severe AS. A threshold of 1651 AU provided the best combination of sensitivity (80%) and specificity (87%) [73].

Even though CT guarantees superior spatial resolution, current clinical guidelines do not recommend CT scans for the diagnosis of AS. This is because CT can only provide the GOA of the valve and cannot provide any hemodynamic data such as ΔP or CO in isolation. Given this, EOA cannot be calculated by using CT. Furthermore there is a discrepancy in scientific studies regarding the existence of strong correlations between the amount of AV calcifications and the severity of the stenosis [74] , or its absence [75, 76], which may happen because AV calcifications only accounts for leaflet mobility and not AV full physiology, i.e. area, CO and flow rate. Also, CT scans involve exposure to x-ray radiation. Cardiologist may s may prefer other noninvasive imaging tools to assess AV functionality.

Despite the findings, CT still provides high spatial resolution data that may be necessary for certain applications which focus on cardiovascular anatomy. Additionally, CT is the only

modality that provides non-invasive assessment of AV calcification. Clinical studies have also suggested that AV calcification is a marker for cardiovascular morbidity.[76, 77] Thus, calcium scoring may prove to be an important complement to echocardiographic/catheter evaluation of AS [78].

Although such technology is not used in clinical practice currently, these promising approaches may increase relevance for CT in the diagnostic and follow up of AS.

5.1.4. Magnetic Resonance Imaging

Two-dimensional phase-contrast MR imaging can be used to calculate the blood flow velocity in a given region of interest (ROI) by measuring the acquired shift in phase of moving protons, as already explained above.[79] If the through-plane velocity across the AV is measured, the pressure gradient (ΔP) across a stenotic valve can be estimated by using the simplified Bernoulli equation (Equation 2.1)

Flow volume across the AV also can be measured by defining an ROI at the level of the AV, multiplying the flow velocity within each pixel in the ROI by the area of the pixel, and summing the results obtained for all pixels in the ROI (Equation 4.2).

$$Flow\ Volume = \sum(V_{\text{pixel}}.\ A_{\text{pixel}}) \qquad (5.5)$$

Alternatively, the flow volume may be obtained by multiplying the average velocity in an ROI (v_{mean}) by the area of the ROI (A_{ROI}) (Equation 4.3).

$$Flow\ Volume = v_{mean}.A_{ROI} \qquad (5.6)$$

From these methods described, it is possible to also obtain the aortic regurgitant volume and consequently the regurgitant fraction [80].

Although flow velocities obtained with phase-contrast MR imaging have been shown to be accurate in phantoms [81, 82], results of PC MRI in vivo may vary because of eddy currents [83, 84], other technical parameters such as phase and VENC, that were described in sections 1.3.3 and 1.3.4, the imaging system and scanning protocol used and the patient scanned. Phasecontrast MR imaging therefore may be more useful for comparing relative flow velocities and volumes within a patient than for comparing absolute flow velocities and volumes between patients.

As already described in the 1.3.3. subchapter, phase-contrast MR imaging also can be used to demonstrate blood flow in three dimensions over time (four-dimensional (4D) flow measurement). When this method is used, flow patterns in the aorta can be displayed and characterized, allowing assessment of the physiologic effects of valvular disease on flow. Aortic stenosis and regurgitation result in turbulent flow. Intravoxel areas of turbulent flow will produce signal voids, which appear as dark “jets” emerging from the valve, in the MR image. These jets are helpful in diagnosing aortic stenosis and regurgitation. However, the magnitude of a jet cannot be encountered as a quantitative indicator of the severity of the stenosis or regurgitation, since it depends on different factors, including the TE, flip angle, and imaging plane [85, 86]. A bicuspid AV, for example, may produce either a normal flow pattern or an eccentric pattern that places greater stress on the aortic wall [87, 88]. Almost no information is available about prognosis for patients with AvD using 4D flow measurement, but this technique

has already shown that is very promising in terms of assessing AV anatomy, physiology and hemodynamics.

5.2. Methods

A total of n=4 AvD patients (n=1 male, n=3 female, age range 17 to 36 years, mean age 27±7 years), that had clinical indications for cardiac catheterization based on Echo, were included. All the patients enrolled have AVS.

Two methods were implemented to assess the pressure gradient in the AV: MRI-based Gorlin Area equation and TCPM from MRI.

The Gorlin Area method is based on Equation 5.2. Using GTFlow (Fraunhofer MEVIS, Bremen, Germany), is possible to create a new plane, perpendicular to the AV, create a ROI in the valve region, analyze the blood flow that goes through it, and export velocity, area, relative pressure and net flow values.

The TCPM method and is described in chapter 4.2.2. However, since in this section we are dealing with AVS and not CoA, the two ROIs chosen were in the LV and Aorta, right before and after the AV, respectively. Also, the aorta segmentation was limited to the AV region, since the information in that region is the only necessary (Figure 18).

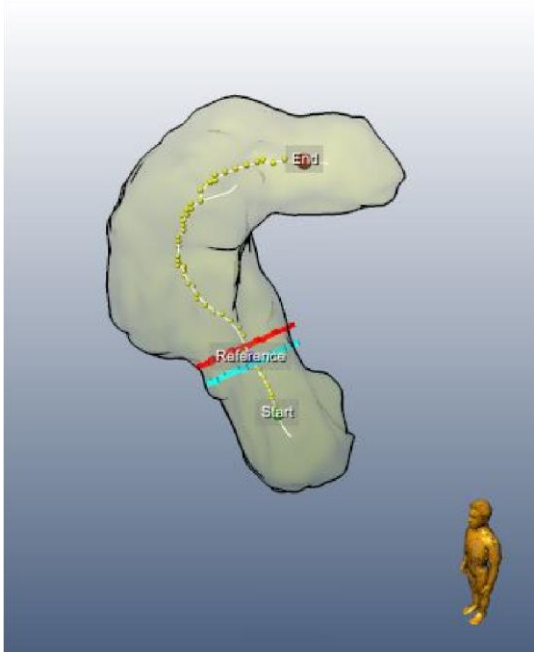

Figure 18 – Aortic Valve mask with the regions of interest and the Start, End and Reference points chosen. It is considered the aortic valve as the reference point.

5.3. Results

The patient characteristics, hemodynamic baseline measurements and MRI measurements are given in Table 4.

Per the power test, the sample size necessary to compare catheter and MRI measurements is 27 patients, which is higher than the number of patients considered (n=4).

The TOST procedure indicated a $p<0.05$, thus the null hypothesis - the population means differ – is rejected, and the two populations can be considered practically equivalent.

Table 4 - Patients characteristics and values of absolute and relative pressure gradients obtained via catheter and MRI.

Patient	Sex	Age (years)	Percentage of flow through the narrowing (%)	Peak-to-Peak Pressure Gradient (Catheter) [mmHg]	Time Shift Corrected Pressure gradient (MRI) [mmHg]	Pressure gradient (Gorlin) [mmHg]
1	F	17	81.60	49.62	57.13	32.76
2	F	36	108.78	16.36	22.85	14.68
3	M	25	63.94	9.68	10.28	4.52
4	F	28	84.61	7.85	8.73	5.92
Mean Value ± Standard Deviation	-	27±7	84.60±18.65	20.88±19.51	24.75±22.50	14.47±13.00

From the Bland-Altman approach is possible to verify the agreement between catheterization (20.88±19.51mHg), TCPM (24.75±22.50 mmHg) and Gorlin Area method (14.47±13.00 mmHg) pressure gradients.

Comparing catheterization and time shift corrected pressure gradients, the bias (mean of differences) was -3.87 mmHg and the limit of agreement (double of the standard deviation) was ±3.64 mmHg (Figure 19). The correlation coefficient between catheterization and TCPM measurements is 0.99 (Figure 21). The linear correlation equation is $CMR = 1.15 Catheterization + 0.79$.

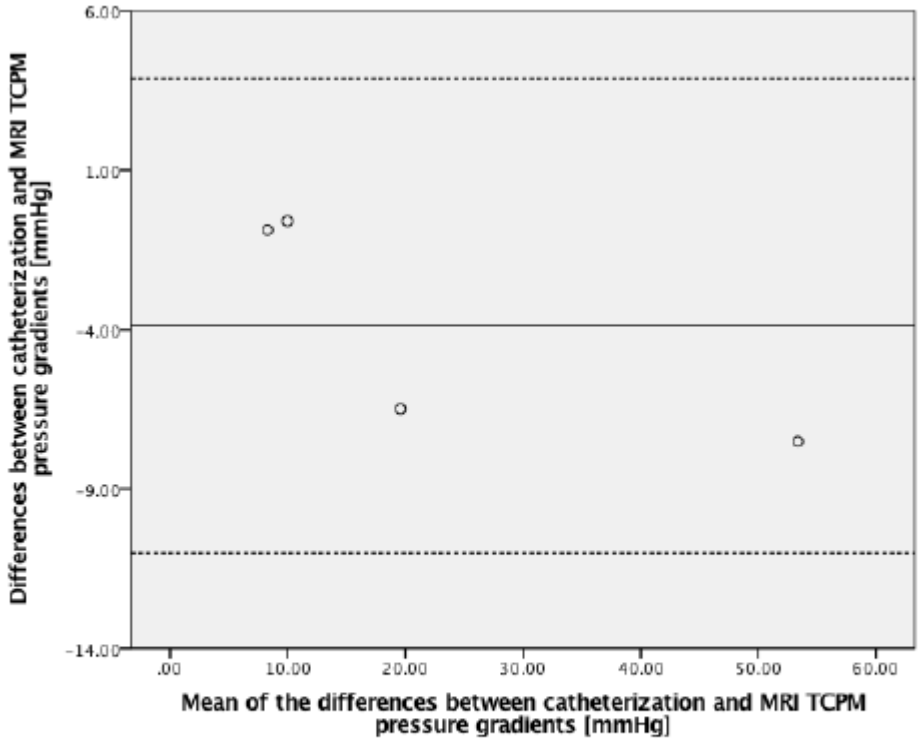

Figure 19 - Bland Altman analysis to compare catheterization and time shift corrected pressure gradients in patients with AS. The bias is -3.87 mmHg and the limit of agreement is ±7.13 mmHg.

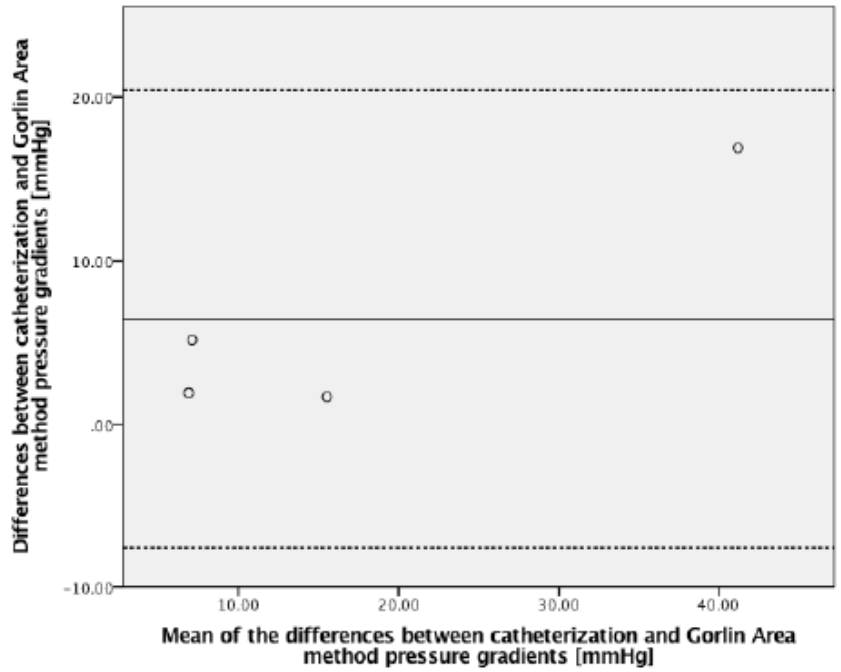

Figure 20 - Bland Altman analysis to compare catheterization and Gorlin Area method pressure gradients, in patients with AS. The bias is 6.41 mmHg and the limit of agreement is ±7.15 mmHg.

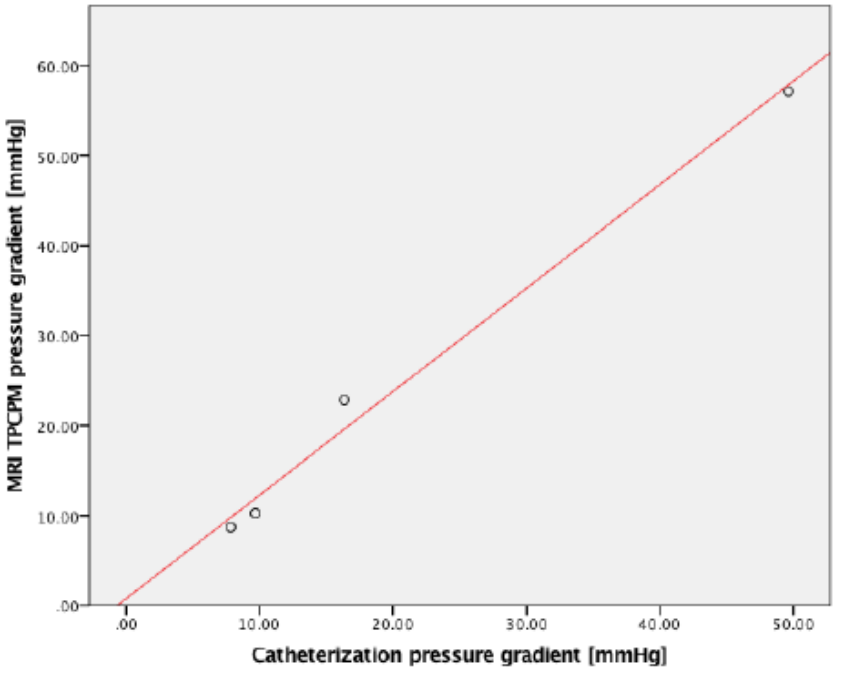

Figure 21 - Scatterplot of the measurements from catheterization and time shift corrected pressure gradients in mmHg, in patients with AS. The red line is the trend line of the linear correlation between the two methods. The correlation coefficient between both absolute measures (catheter and MRI) is 0.99. The correlation equation is $\boldsymbol{CMR = 1.15\,Catheterization + 0.79}$

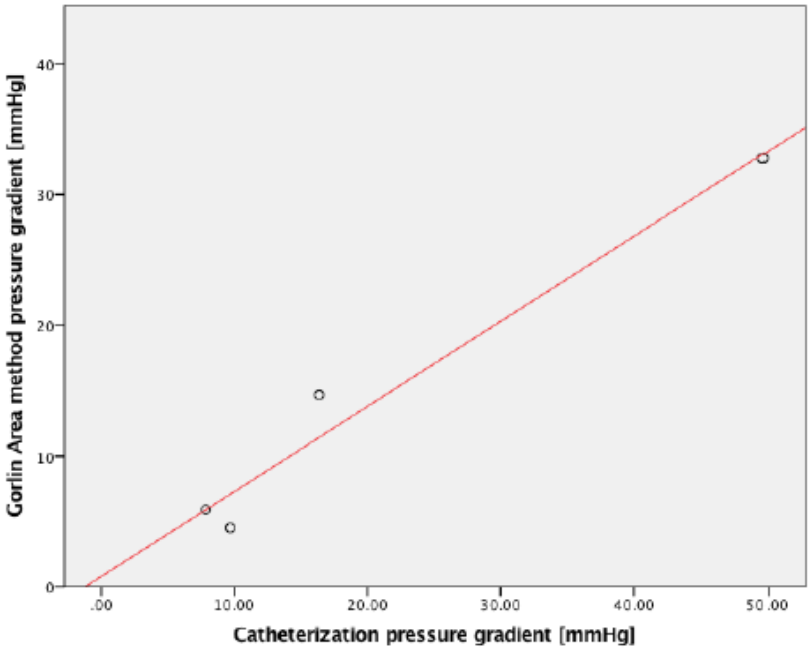

Figure 22 - Scatterplot of the measurements from catheterization and Gorlin Area method pressure gradients, in mmHg, in patients with AS The red line is the trend line of the linear correlation between the two methods. The correlation coefficient between both absolute measures (catheter and MRI) is 0.97. The correlation equation is $\boldsymbol{CMR = 0.65\ Catheterization + 0.80}$

Comparing catheterization and Gorlin Area method pressure gradients, the bias is 6.41 mmHg and the limit of agreement is ±7.15 mmHg (Figure 21). The correlation coefficient between both measures (catheterization and Gorlin Area method) is 0.97 (Figure 22). The linear correlation equation is $CMR = 0.65 \quad Catheterization + 0.80$.

5.4. Discussion

The described study presents a non-invasive MRI based method for time-shift corrected CoA pressure gradient applied to AvD patients. Measurements were performed in a small group of AvD patients with peak-to-peak pressure gradient values very scattered. The results show a good agreement between TCPM (24.75±22.50 mmHg), the Gorlin Area method (14.47±13.00 mmHg) and catheter derived peak-to-peak pressure gradients (20.88±19.51 mmHg), in AvD patients, more specifically AVS patients.

As already mentioned in Section 1.2.2, for AVS patients, early therapy is strongly advised and intervention is recommended for patients with severe AVS and DP ≥ 40 mmHg.

Currently available tools to measure non-invasively the pressure gradient are not always reliable. From Doppler Echocardiography, it is possible to measure AV mean gradient. However, this measure is not the best marker of the severity of AS since it is dependent on the aortic valve area (AVA), which is not easily measured and can have different values for different technicians measuring. CT guarantees superior spatial resolution. However, it can only provide the GOA of the valve and cannot provide any hemodynamic data such as ΔP or CO in isolation, useful for the proper diagnosis of AvD.

From Phase-Contrast MR imaging, it is possible to obtain accurately flow velocities in phantoms [89, 90]. However, results of PC MRI in vivo may vary because of eddy currents [91, 92], other technical parameters as phase and VENC, that were described in sections 2.3.3 and 2.3.4, the

imaging system and scanning protocol used and the patient scanned. Because of these dependencies, phase-contrast MR imaging may be more useful for comparing relative flow velocities and volumes within a patient than for comparing absolute flow velocities and volumes between patients.

The Gorlin Area method, introduced in the section 5.1 and compared with catheterization, tends to slightly underestimate the pressure gradients. The selection of the GOA is manual and may change from person to person. This aspect gives a great degree of uncertainty to this method and shows that is not a method clinically reliable. These statements agree with our results.

The TCPM allows non-invasive measurement of the absolute pressure gradients, using the relative pressure gradient and pressure variation over time in the aortic valve. When applied to AvD, the choice of the ROIs was more challenging. The goal was to compare regions right before and after the valve, so the ROIs chosen were very close together. The pressure gradient may vary if there is increased turbulence, due to the malformation in the valve, which can explain the slight overestimation of the TPCM method [63].

In the cohort of analyzed patients, one had severe AVS and the remaining had moderate AVS, under typical clinical setting conditions. As already happened in the first study, three patients had clinical indication for cardiac catheterization without having a pressure gradient exceeding 30 mmHg. These cases reinforce the need for an improved diagnostic workup to avoid invasive procedures in non-borderline cases.

5.5. Limitations and Future Work

Our cohort of 4 patients only contemplates AVS patients and is not sufficient to validate the TCPM method in AVD patients. Bigger cohorts with AVS and AVR patients are advised to understand the method and understand if optimization is needed. Also, further evaluation in multicentre studies would be helpful to promote more confidence in the new method.

The ROIs must be normal to the blood flow. Using MevisFlow, this choice is not easy, since it depends on the perspective of each user. It would be a great improvement if the software could get the direction information from the velocity fields, and could automatically put the ROIs normal to the blood flow.

6. Conclusion

This work intends to develop and test a method to non-invasively measure the absolute pressure gradients in COA and AvD patients. Evaluating and predicting relevant parameters is fundamental to diagnose the diseases at an early stage and prevent further evolution. Giving this, it is necessary to test and validate new assessment techniques.

The TCPM method proposed in this study allows a fully non-invasive semi-automated, patient and user-friendly assessment in using relative pressure maps. Several aspects must be considered by clinicians to ensure the accuracy of the method. Since net flow is an indicator of the aortic pulse wave, the time points of maximal flow rate, in the ascending and descending aorta/before and after aortic valve, were considered as markers for the time-shift [98]. Accordingly, the ROIs have to be carefully placed orthogonally to the main flow direction in the aorta for obtaining proper flow and velocity mean values, as well as relative pressures [57].

These present studies show the direct comparison between catheterization and two non-invasive methods: TCPM and Doppler Echocardiography, in the first study, TCPM and Gorlin Area method, in the second study. In conformity with the literature review made, the Doppler Echocardiography overestimated the catheterization values, and the Gorlin Area method underestimated the catheterization values. Given the obtained results, in future research, it should be possible to prioritize TPCM method over other non-invasive methods, but most importantly, over catheterization. Moreover, in the future, additional developments and research need to be done concerning AvD, since the cohort was only constituted by 4 patients and all the patients had AVS, meaning the method was not tested in AVR patients.

The key feature of the method described is improving the CoA and AvD diagnostic by being a tool of intervention decision-making before any invasive technique is used. This methodology has the potential to be incorporated in clinical routine. Future studies would be recommended to evaluate this technique in other cardiovascular stenosis diseases.

Bibliography

[1] W. H. O. (WHO). (Updated May 2017, 03/07/2017). *Cardiovascular diseases (CVDs)*.

[2] H. Baumgartner *et al.*, "ESC Guidelines for the management of grown-up congenital heart disease (new version 2010)The Task Force on the Management of Grown-up Congenital Heart Disease of the European Society of Cardiology (ESC)," *European Heart Journal*, vol. 31, no. 23, pp. 2915-2957, 2010.

[3] E. J. Dijkema, T. Leiner, and H. B. Grotenhuis, "Diagnosis, imaging and clinical management of aortic coarctation," *Heart*, 2017.

[4] H. Markel *et al.*, "Exercise-induced hypertension after repair of coarctation of the aorta: Arm versus leg exercise," *Journal of the American College of Cardiology*, vol. 8, no. 1, pp. 165-171, 1986/07/01/ 1986.

[5] L. A. Marks and A. Groch, "Optimizing cuff width for noninvasive measurement of blood pressure," *Blood Pressure Monitoring*, vol. 5, no. 3, pp. 153-158, 2000.

[6] L. L. M. Wyman W. Lai, Meryl S. Cohen, Tal Geva *Echocardiography in Pediatric and Congenital Heart Disease: From Fetus to Adult*, 2nd ed. 2016.

[7] J. N. Oshinski *et al.*, "Improved Measurement of Pressure Gradients in Aortic Coarctation by Magnetic Resonance Imaging," *Journal of the American College of Cardiology*, vol. 28, no. 7, pp. 1818-1826, 1996/12/01/ 1996.

[8] E. Riesenkampff *et al.*, "Pressure fields by flow-sensitive, 4D, velocity-encoded CMR in patients with aortic coarctation," *J Am Coll Cardiol Img*, vol. 7, no. 9, pp. 920-6, Sep 2014.

[9] W. E. Arnould-Taylor, *A Textbook of Anatomy and Physiology*, 3rd ed. Nelson Thomes, 1998.

[10] J. P. T. W. Philip I. Aaronson, Michelle J. Connolly, *The Cardiovascular System at a Glance*, 4th ed. Wiley-Blackwell, 2012.

[11] B. A. Carabello, "Introduction to Aortic Stenosis," *Circulation Research*, vol. 113, no. 2, pp. 179-185, 2013.

[12] H. Baumgartner *et al.*, "ESC Guidelines for the management of grown-up congenital heart disease (new version 2010)," (in eng), *Eur Heart J*, vol. 31, no. 23, pp. 2915-57, Dec 2010.

[13] T. J. Forbes *et al.*, "Comparison of surgical, stent, and balloon angioplasty treatment of native coarctation of the aorta: an observational study by the CCISC (Congenital Cardiovascular Interventional Study Consortium)," (in eng), *J Am Coll Cardiol*, vol. 58, no. 25, pp. 2664-74, Dec 13 2011.

[14] C. Zabal, F. Attie, M. Rosas, A. Buendia-Hernandez, and J. A. Garcia-Montes, "The adult patient with native coarctation of the aorta: balloon angioplasty or primary stenting?," (in eng), *Heart*, vol. 89, no. 1, pp. 77-83, Jan 2003.

[15] E. Riesenkampff *et al.*, "Pressure fields by flow-sensitive, 4D, velocity-encoded CMR in patients with aortic coarctation," (in eng), *JACC Cardiovasc Imaging*, vol. 7, no. 9, pp. 920-6, Sep 2014.

[16] N. Saikrishnan, G. Kumar, F. J. Sawaya, S. Lerakis, and A. P. Yoganathan, "Accurate Assessment of Aortic Stenosis," *Circulation*, vol. 129, no. 2, pp. 244-253, 2014.

[17] C. M. Otto *et al.*, "Prospective Study of Asymptomatic Valvular Aortic Stenosis," *Clinical, Echocardiographic, and Exercise Predictors of Outcome*, vol. 95, no. 9, pp. 2262-2270, 1997.

[18] M. M. Elahi, A. Chuang, M. J. Ewing, C. H. Choi, P. W. Grant, and B. M. Matata, "One problem two issues! Left ventricular systolic and diastolic dysfunction in aortic stenosis," *Annals of Translational Medicine*, vol. 2, no. 1, p. 10.

[19] H. Baumgartner *et al.*, "Echocardiographic assessment of valve stenosis: EAE/ASE recommendations for clinical practice," *European Journal of Echocardiography*, vol. 10, no. 1, pp. 1-25, 2009.

[20] D. T. Ginat, M. W. Fong, D. J. Tuttle, S. K. Hobbs, and R. C. Vyas, "Cardiac Imaging: Part 1, MR Pulse Sequences, Imaging Planes, and Basic Anatomy," *American Journal of Roentgenology*, vol. 197, no. 4, pp. 808-815, 2011/10/01 2011.

[21] E. M. Haacke and G. W. Lenz, "Improving MR image quality in the presence of motion by using rephasing gradients," *American Journal of Roentgenology*, vol. 148, no. 6, pp. 1251-1258, 1987/06/01 1987.

[22] J. Lotz, C. Meier, A. Leppert, and M. Galanski, "Cardiovascular flow measurement with phasecontrast MR imaging: basic facts and implementation," (in eng), *Radiographics*, vol. 22, no. 3, pp. 651-71, May-Jun 2002.

[23] B. Schulte, A. Boldt, and D. Beyer, *MRT des Herzens und der Gefäße*. 2005.

[24] M. B. Srichai, R. P. Lim, S. Wong, and V. S. Lee, "Cardiovascular applications of phasecontrast MRI," (in eng), *AJR Am J Roentgenol*, vol. 192, no. 3, pp. 662-75, Mar 2009.

[25] E. A.D. (2017, June 8th). *MR Artifacts - Why does the phase wrap-around artifact occur?*

[26] M. a. K. W. J. Jack L. Cronenwett, MD, FRCSC, *Rutherford's Vascular Surgery*. 2014.

[27] (in - eng), no. - 0009-7322 (Print).

[28] B. Baccani, F. Domenichini, and G. Pedrizzetti, *Model and influence of mitral valve opening during the left ventricular filling*. 2003, pp. 355-61.

[29] K. Balachandran, P. Sucosky, and A. P. Yoganathan, "Hemodynamics and Mechanobiology of Aortic Valve Inflammation and Calcification," *International Journal of Inflammation*, vol. 2011, p. 263870.

[30] B. J. Bellhouse, "Fluid mechanics of a model mitral valve and left ventricle1," *Cardiovascular Research*, vol. 6, no. 2, pp. 199-210, 1972.

[31] C. Yellin El Fau - Peskin *et al.*, "Mechanisms of mitral valve motion during diastole," (in eng), no. 0002-9513 (Print), 19811118 DCOM- 19811118.

[32] B. Schulte, A. Boldt, and D. Beyer, *MRT des Herzens und der Gefäße*. 2005.

[33] A. B. Golden and W. E. Hellenbrand, "Coarctation of the aorta: Stenting in children and adults," *Catheterization and Cardiovascular Interventions*, vol. 69, no. 2, pp. 289-299, 2007.

[34] G. W. Forrester JS, Diamond G, McHugh T, Chonette DW, Swan HJ., "Thermodilution cardiac output determination with a single flow-directed catheter," 1972

[35] P. R. Vale *et al.*, "Randomized, Single-Blind, Placebo-Controlled Pilot Study of Catheter-Based Myocardial Gene Transfer for Therapeutic Angiogenesis Using Left Ventricular Electromechanical Mapping in Patients With Chronic Myocardial Ischemia," *Circulation*, vol. 103, no. 17, pp. 2138-2143, May 1, 2001 2001.

[36] A. B. Houston, Simpson, I.A., Pollock, J.C, "Doppler ultrasound in the assessment of severity of coarctation of the aorta and interruption of the aortic arch," 1987.

[37] T. G. D. Abdul W. Aldousany, Bruce S. Alpert, Stuart E. Birnbaum, and Elaine S. Willey, "Significance of the Doppler-Derived Gradient Across a Residual Aortic Coarctation," *Pediatric Cardiology*, vol. 11, no. 1, pp. 8-14, 1990.

[38] A. P. Yoganathan *et al.*, "Continuous-wave Doppler velocities and gradients across fixed tunnel obstructions: studies in vitro and in vivo," *Circulation*, vol. 76, no. 3, pp. 657-666, 1987.

[39] J. N. Oshinski *et al.*, "Improved Measurement of Pressure Gradients in Aortic Coarctation by Magnetic Resonance Imaging," *Journal of the American College of Cardiology*, vol. 28, no. 7, pp. 1818-1826, 1996.

[40] M. H. R. Nyman, J. Sunnegardh, J. Thurén and A. Henze, "Magnetic Resonance Imaging and Angiography for the Assessment of Coarctation of the Aorta," *Acta Radiologica*, vol. 30, pp. 481-485, 1989.

[41] I. A. Simpson, K. J. Chung, R. F. Glass, D. J. Sahn, F. S. Sherman, and J. Hesselink, "Cine magnetic resonance imaging for evaluation of anatomy and flow relations in infants and children with coarctation of the aorta," *Circulation*, vol. 78, no. 1, pp. 142-148, 1988.

[42] H. C. Stern *et al.*, "Noninvasive assessment of coarctation of the aorta: Comparative measurements by two-dimensional echocardiography, magnetic resonance, and angiography," *Pediatric Cardiology*, journal article vol. 12, no. 1, pp. 1-5, 1991.

[43] J. A. Sotelo *et al.*, "Pressure gradient prediction in aortic coarctation using a computationalfluid-dynamics model: validation against invasive pressure catheterization at rest and pharmacological stress," *Journal of Cardiovascular Magnetic Resonance*, journal article vol. 17, no. 1, p. Q78, 2015.

[44] S. Jain, F. J. Londono, P. Segers, T. C. Gillebert, M. De Buyzere, and J. A. Chirinos, "MRI Assessment of Diastolic and Systolic Intraventricular Pressure Gradients in Heart Failure," *Current Heart Failure Reports*, journal article vol. 13, no. 1, pp. 37-46, 2016.

[45] M. Markl, P. J. Kilner, and T. Ebbers, "Comprehensive 4D velocity mapping of the heart and great vessels by cardiovascular magnetic resonance," *Journal of Cardiovascular Magnetic Resonance*, vol. 13, no. 1, pp. 7-7, 01/14

[46] M. W. a. H.-C. H. Detlev Stalling, "Amira - a Highly Interactive System for Visual Data Analysis," (The Visualization Handbook. Elsevier, 2005, p.^pp. Pages.

[47] S. Meier, A. Hennemuth, J. Drexl, J. Bock, B. Jung, and T. Preusser, "A Fast and Noise-Robust Method for Computation of Intravascular Pressure Difference Maps from 4D PC-MRI Data," in *Statistical Atlases and Computational Models of the Heart. Imaging and Modelling Challenges: Third International Workshop, STACOM 2012, Held in Conjunction with MICCAI 2012, Nice, France, October 5, 2012, Revised Selected Papers*, O. Camara, T. Mansi, M. Pop, K. Rhode, M. Sermesant, and A. Young, Eds. Berlin, Heidelberg: Springer Berlin Heidelberg, 2013, pp. 215-224.

[48] M. F. Salfity, J. M. Huntley, M. J. Graves, O. Marklund, R. Cusack, and D. A. Beauregard, "Extending the dynamic range of phase contrast magnetic resonance velocity imaging using advanced higher-dimensional phase unwrapping algorithms," *Journal of The Royal Society Interface*, vol. 3, no. 8, pp. 415-427, 2006.

[49] S. Meier, A. Hennemuth, O. Friman, J. Bock, M. Markl, and T. Preusser, "Non-invasive 4D blood flow and pressure quantification in central blood vessels via PC-MRI," in *2010 Computing in Cardiology*, 2010, pp. 903-906: IEEE.

[50] S. Meier, A. Hennemuth, J. Drexl, J. Bock, B. Jung, and T. Preusser, "A fast and noise-robust method for computation of intravascular pressure difference maps from 4D PC-MRI Data," in *International Workshop on Statistical Atlases and Computational Models of the Heart*, 2012, pp. 215-224: Springer.

[51] B. Lautrup, *Physics of Continuous Matter - Exotic and Everyday Phenomena in the Macroscopic World*. London: Institute of Physics Publishing, 2005.

[52] G. M. London and A. P. Guerin, "Influence of arterial pulse and reflected waves on blood pressure and cardiac function," *American Heart Journal*, vol. 138, no. 3, pp. S220-S224, 1999/09/01/ 1999.

[53] J. M. Bland and D. G. Bland, "Statistics Notes: One and two sided tests of significance," *BMJ*, vol. 309, no. 6949, p. 248, 1994.

[54] F. Faul, E. Erdfelder, A. G. Lang, and A. Buchner, "G*Power 3: a flexible statistical power analysis program for the social, behavioral, and biomedical sciences," (in eng), *Behav Res Methods*, vol. 39, no. 2, pp. 175-91, May 2007.

[55] P. A. Iaizzo, *Handbook of Carciac Anatomy, Physiology, and Devices*. Humana Press, 2005.

[56] L. Tang, T. J. Forbes, W. Du, and M. V. Zilberman, "Echocardiographic evaluation of pressure gradient across the stent in patients treated for coarctation of the aorta," (in eng), *Congenit Heart Dis,* vol. 4, no. 4, pp. 269-72, Jul-Aug 2009.

[57] P. Lamata *et al.*, "Aortic Relative Pressure Components Derived from Four-Dimensional Flow Cardiovascular Magnetic Resonance," *Magn Reson Med,* vol. 72, no. 4, pp. 1162-9, Oct 2014.

[58] K. R. O'Brien, B. R. Cowan, M. Jain, R. A. Stewart, A. J. Kerr, and A. A. Young, "MRI phase contrast velocity and flow errors in turbulent stenotic jets," (in eng), *J Magn Reson Imaging,* vol. 28, no. 1, pp. 210-8, Jul 2008.

[59] M. Kelm *et al.*, "MRI as a tool for non-invasive vascular profiling: a pilot study in patients with aortic coarctation," (in eng), *Expert Rev Med Devices,* vol. 13, no. 1, pp. 103-12, 2016.

[60] D. Garcia, Kadem, Lyes, "What Do You Mean by Aortic Valve Area: Geometric Orifice Area, Effective Orifice Area, or Gorlin Area?," *The Journal of Heart Valve Disease,* vol. 15, no. 5, pp. 601-608, 2006.

[61] G. K. Batchelor, *An introduction to fluid dynamics*. Cambridge: Cambridge University Press, 1967.

[62] N. Saikrishnan, G. Kumar, F. J. Sawaya, S. Lerakis, and A. P. Yoganathan, "Accurate Assessment of Aortic Stenosis," *Circulation,* 10.1161/CIRCULATIONAHA.113.002310 vol. 129, no. 2, p. 244, 2014.

[63] B. Schulte, A. Boldt, and D. Beyer, *MRT des Herzens und der Gefäße*. 2005.

[64] P. Pibarot and J. G. Dumesnil, "New concepts in valvular hemodynamics: Implications for diagnosis and treatment of aortic stenosis," *The Canadian Journal of Cardiology,* vol. 23, no. Suppl B, pp. 40B-47B, 2007.

[65] J. D. Thomas, J. B. Newell, C. Y. Choong, and A. E. Weyman, "Physical and physiological determinants of transmitral velocity: numerical analysis," (in eng), *Am J Physiol,* vol. 260, no. 5 Pt 2, pp. H1718-31, May 1991.

[66] S. H. Rahimtoola, A. Durairaj, A. Mehra, and I. Nuno, "Current Evaluation and Management of Patients With Mitral Stenosis," *Circulation,* vol. 106, no. 10, pp. 1183-1188, 2002.

[67] R. O. Bonow *et al.*, "2008 focused update incorporated into the ACC/AHA 2006 guidelines for the management of patients with valvular heart disease: a report of the American College of Cardiology/American Heart Association Task Force on Practice Guidelines (Writing Committee to revise the 1998 guidelines for the management of patients with valvular heart disease). Endorsed by the Society of Cardiovascular Anesthesiologists, Society for Cardiovascular Angiography and Interventions, and Society of Thoracic Surgeons," (in eng), *J Am Coll Cardiol,* vol. 52, no. 13, pp. e1-142, Sep 23 2008.

[68] M. Engoren and D. Barbee, "Comparison of cardiac output determined by bioimpedance, thermodilution, and the Fick method," (in eng), *Am J Crit Care,* vol. 14, no. 1, pp. 40-5, Jan 2005.

[69] R. Gorlin and S. G. Gorlin, "Hydraulic formula for calculation of the area of the stenotic mitral valve, other cardiac valves, and central circulatory shunts. I," (in eng), *Am Heart J,* vol. 41, no. 1, pp. 1-29, Jan 1951.

[70] A. H. Hakki *et al.*, "A simplified valve formula for the calculation of stenotic cardiac valve areas," *Circulation,* vol. 63, no. 5, pp. 1050-1055, 1981.

[71] K. Nikolaou, H. Alkadhi, F. Bamberg, S. Leschka, and B. J. Wintersperger, "MRI and CT in the diagnosis of coronary artery disease: indications and applications," *Insights into Imaging,* vol. 2, no. 1, pp. 9-24, 2011.

[72] L. Wexler *et al.*, "Coronary Artery Calcification: Pathophysiology, Epidemiology, Imaging Methods, and Clinical Implications," *A Statement for Health Professionals From the American Heart Association,* vol. 94, no. 5, pp. 1175-1192, 1996.

[73] A. S. Agatston, W. R. Janowitz, F. J. Hildner, N. R. Zusmer, M. Viamonte, Jr., and R. Detrano, "Quantification of coronary artery calcium using ultrafast computed tomography," (in eng), *J Am Coll Cardiol,* vol. 15, no. 4, pp. 827-32, Mar 15 1990.

[74] C. Cueff *et al.*, "Measurement of aortic valve calcification using multislice computed tomography: correlation with haemodynamic severity of aortic stenosis and clinical implication for patients with low ejection fraction," (in eng), *Heart,* vol. 97, no. 9, pp. 721-6, May 2011.

[75] P. Pibarot and J. G. Dumesnil, "Improving assessment of aortic stenosis," (in eng), *J Am Coll Cardiol,* vol. 60, no. 3, pp. 169-80, Jul 17 2012.

[76] E. R. Mohler, 3rd, E. Medenilla, H. Wang, and C. Scott, "Aortic valve calcium content does not predict aortic valve area," (in eng), *J Heart Valve Dis,* vol. 15, no. 3, pp. 322-8, May 2006.

[77] S. J. Cowell *et al.*, "Aortic valve calcification on computed tomography predicts the severity of aortic stenosis," (in eng), *Clin Radiol,* vol. 58, no. 9, pp. 712-6, Sep 2003.

[78] G. M. Feuchtner *et al.*, "Aortic valve calcification as quantified with multislice computed tomography predicts short-term clinical outcome in patients with asymptomatic aortic stenosis," (in eng), *J Heart Valve Dis,* vol. 15, no. 4, pp. 494-8, Jul 2006.

[79] R. Rosenhek *et al.*, "Predictors of outcome in severe, asymptomatic aortic stenosis," (in eng), *N Engl J Med,* vol. 343, no. 9, pp. 611-7, Aug 31 2000.

[80] J. F. Glockner, D. L. Johnston, and K. P. McGee, "Evaluation of Cardiac Valvular Disease with MR Imaging: Qualitative and Quantitative Techniques," *RadioGraphics,* vol. 23, no. 1, pp. e9e9, 2003.

[81] J. Lotz, C. Meier, A. Leppert, and M. Galanski, "Cardiovascular Flow Measurement with PhaseContrast MR Imaging: Basic Facts and Implementation," *RadioGraphics,* vol. 22, no. 3, pp. 651-671, 2002.

[82] J. Vogel-Claussen, H. Pannu, P. J. Spevak, E. K. Fishman, and D. A. Bluemke, "Cardiac Valve Assessment with MR Imaging and 64-Section Multi–Detector Row CT," *RadioGraphics,* vol. 26, no. 6, pp. 1769-1784, 2006/11/01 2006.

[83] G. A. Varaprasathan, P. A. Araoz, C. B. Higgins, and G. P. Reddy, "Quantification of Flow Dynamics in Congenital Heart Disease: Applications of Velocity-encoded Cine MR Imaging," *RadioGraphics,* vol. 22, no. 4, pp. 895-905, 2002.

[84] C. J. Bakker, M. Kouwenhoven, M. J. Hartkamp, R. M. Hoogeveen, and W. P. Mali, "Accuracy and precision of time-averaged flow as measured by nontriggered 2D phase-contrast MR angiography, a phantom evaluation," (in eng), *Magn Reson Imaging,* vol. 13, no. 7, pp. 959-65, 1995.

[85] A. Lingamneni, P. A. Hardy, K. A. Powell, N. J. Pelc, and R. D. White, "Validation of cine phase-contrast MR imaging for motion analysis," (in eng), *J Magn Reson Imaging,* vol. 5, no. 3, pp. 331-8, May-Jun 1995.

[86] C. Cueff *et al.*, "Measurement of aortic valve calcification using multislice computed tomography: correlation with haemodynamic severity of aortic stenosis and clinical implication for patients with low ejection fraction," *Heart,* p. hrt. 2010.198853, 2010.

[87] D. Messika-Zeitoun *et al.*, "Evaluation and clinical implications of aortic valve calcification measured by electron-beam computed tomography," *Circulation,* vol. 110, no. 3, pp. 356-362, 2004.

[88] P. D. Gatehouse *et al.*, "Flow measurement by cardiovascular magnetic resonance: a multicentre multi-vendor study of background phase offset errors that can compromise the accuracy of derived regurgitant or shunt flow measurements," (in eng), *J Cardiovasc Magn Reson,* vol. 12, p. 5, Jan 14 2010.

[89] M. P. Rolf *et al.*, "Sequence optimization to reduce velocity offsets in cardiovascular magnetic resonance volume flow quantification--a multi-vendor study," (in eng), *J Cardiovasc Magn Reson,* vol. 13, p. 18, Mar 09 2011.

[90] C. A. Warnes *et al.*, "ACC/AHA 2008 Guidelines for the Management of Adults with Congenital Heart Disease: a report of the American College of Cardiology/American Heart Association Task Force on Practice Guidelines (writing committee to develop guidelines on the management of adults with congenital heart disease)," *Circulation,* vol. 118, no. 23, pp. e714833, Dec 2 2008.

[91] M.-H. Wu, H.-C. Chen, F.-Y. Kao, and S.-K. Huang, "Risk of Systemic Hypertension and Cerebrovascular Accident in Patients With Aortic Coarctation Aged <60 Years (from a National Database Study)," *The American Journal of Cardiology,* vol. 116, no. 5, pp. 779-784, 2015/09/01/ 2015.

[92] Z. Keshavarz-Motamed *et al.*, "Elimination of Transcoarctation Pressure Gradients Has No Impact on Left Ventricular Function or Aortic Shear Stress After Intervention in Patients With Mild Coarctation," *JACC: Cardiovascular Interventions,* vol. 9, no. 18, pp. 1953-1965, 2016/09/26/ 2016.

[93] A. Donti *et al.*, "Frequency of Intracranial Aneurysms Determined by Magnetic Resonance Angiography in Children (Mean Age 16) Having Operative or Endovascular Treatment of Coarctation of the Aorta (Mean Age 3)," *The American Journal of Cardiology,* vol. 116, no. 4, pp. 630-633, 2015/08/15/ 2015.

[94] R. E. Shaddy *et al.*, "Comparison of angioplasty and surgery for unoperated coarctation of the aorta," *Circulation,* vol. 87, no. 3, pp. 793-799, 1993.

[95] D. Tanous, L. N. Benson, and E. M. Horlick, "Coarctation of the aorta: evaluation and management," *Curr Opin Cardiol,* vol. 24, no. 6, pp. 509-15, Nov 2009.

[96] M. G. Dellborg, M. Astengo, C. Berntsson, P. Eriksson, and V. Fisichella, "Ability of the european sociaty of cardiology guidelines to predict heamodynamically significant coarctation of the aorta," *Journal of the American College of Cardiology,* vol. 61, no. 10, p. E554, 2013.

[97] M. Kelm *et al.*, "MRI as a tool for non-invasive vascular profiling: a pilot study in patients with aortic coarctation," *Expert Rev Med Devices,* vol. 13, no. 1, pp. 103-12, 2016.

[98] V. A. Raimund Erbel, Catherine Boileau, Eduardo Bossone,, H. E. Roberto Di Bartolomeo, Arturo Evangelista, Volkmar Falk,, O. G. Herbert Frank, Martin Grabenwöger, Axel Haverich, Bernard, and A. J. M. Iung, "2*014 ESC Guidelines on the diagnosis and treatment of aortic diseases*" *European Heart Journal,* vol. 37, no. 46, pp. 35-41, 2014.

[99] Z. Stankovic, B. D. Allen, J. Garcia, K. B. Jarvis, and M. Markl, "4D flow imaging with MRI," *Cardiovascular Diagnosis and Therapy,* vol. 4, no. 2, pp.

[100] M. A. Clavel, "Echocardiographic Assessment of Aortic Stenosis Severity: Do Not Rely on a Single Parameter," *Journal of the American Heart Association: Cardiovascular and Cerebrovascular Disease,* vol. 5, no. 10, p. e004680, 10/22 2016.

[101] M. D. Hope *et al.*, "4D flow CMR in assessment of valve-related ascending aortic disease," (in eng), *JACC Cardiovasc Imaging,* vol. 4, no. 7, pp. 781-7, Jul 2011.

Annex I – Segmentation mask of the 27 CoA patients.

In this annex, the masks of the aorta of each patient are present. The rings represent the ROIs chosen for each case. There is always one ROI in the ascending aorta, and a second ROI in the descending aorta. The ROIs must be normal to the blood flow. The start, end and reference points for the centerline relative pressure map computation are defined in all masks. The reference point is near the brachiocephalic artery, to not consider the flow turbulence, typical from the valve region, and the flow turbulence that may occur due the narrowing.

1 **2** **3** **4** **5**

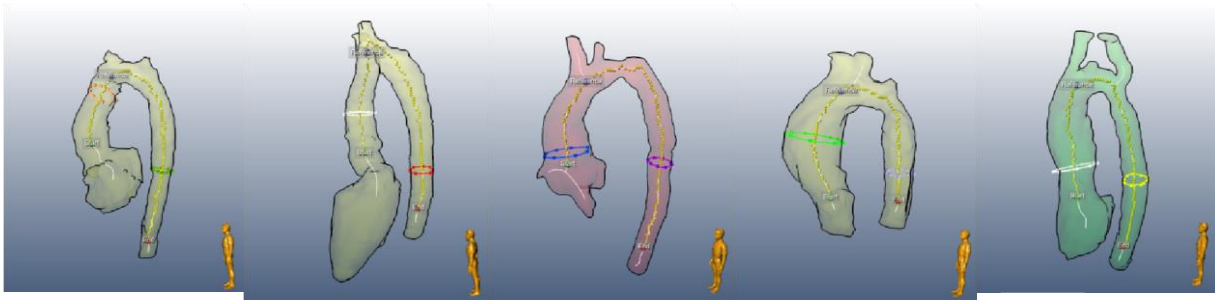

6 **7** **8** **9** **10**

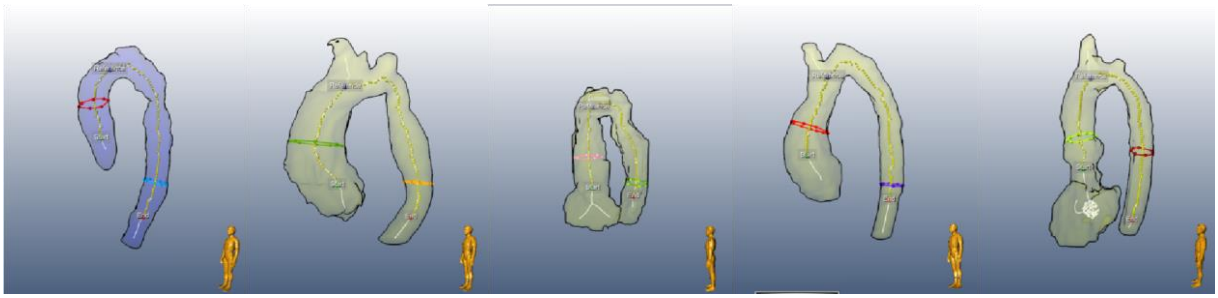

11 **12** **13** **14** **15**

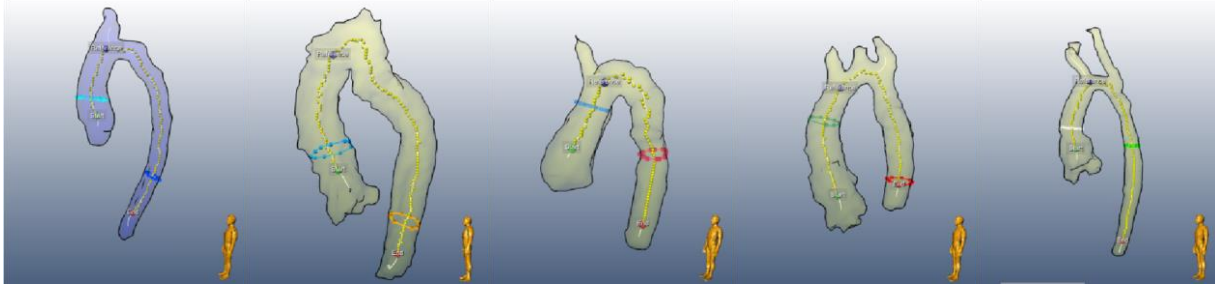

16 **17** **18** **19** **20**

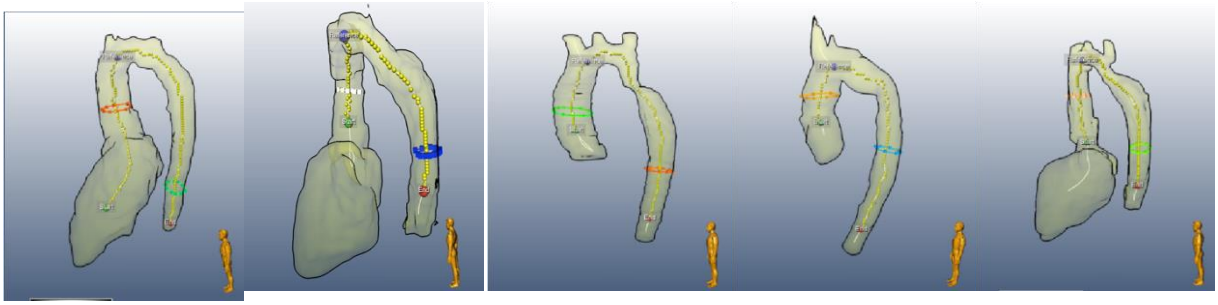

21

22

23

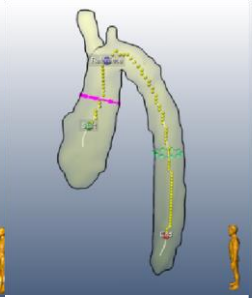

24

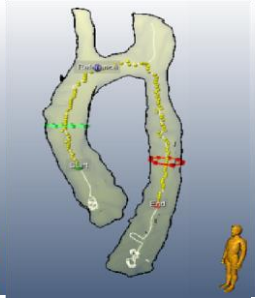

25

26

27

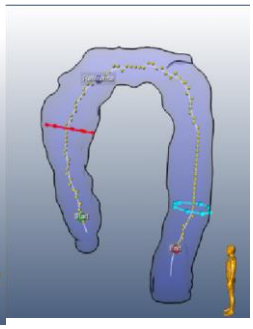

Annex II – Relative pressure maps of the 27 CoA patients.

Centerline relative pressure maps computation results from the masks presented in Annex I. The scale of each patient is present on the left side of each image, and it differs from patient to patient. The red color is associated with positive pressure gradients and the blue color is associated with negative pressure gradients. All these images were collected in the time-point in which the relative pressure gradient between the ROIs chosen was bigger.

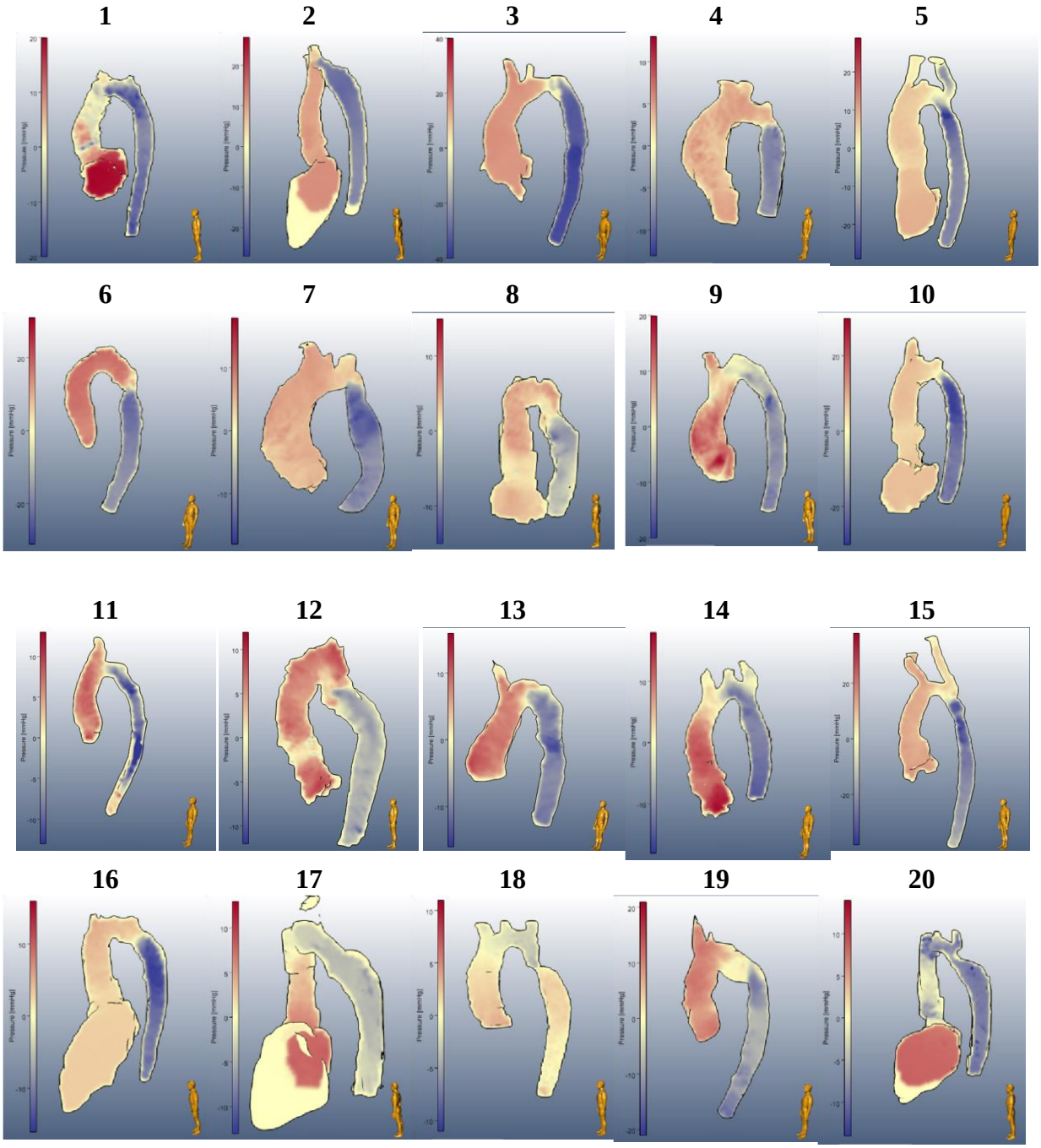

21

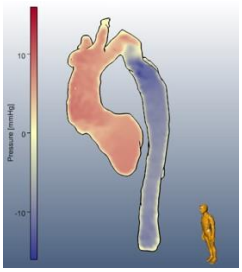

22

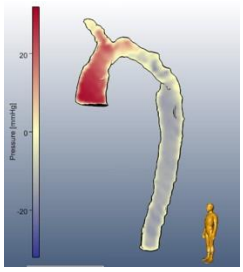

23

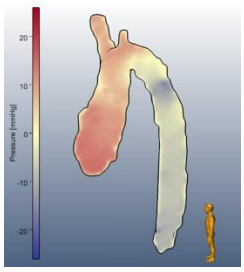

24

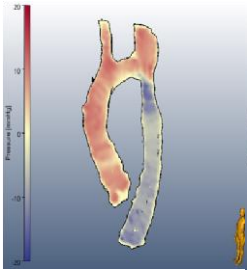

25

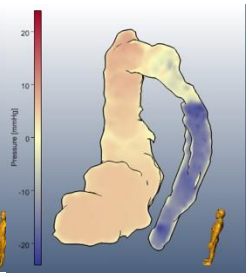

26

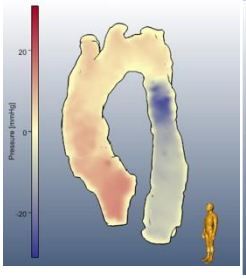

27